

# COLUMBIA UNIVERSITY

IN THE CITY OF NEW YORK

SCHOOL OF ENGINEERING AND APPLIED SCIENCE

ELECTRONICS RESEARCH LABORATORIES

## ELECTRO-OPTICAL SIGNAL PROCESSING TECHNIQUES

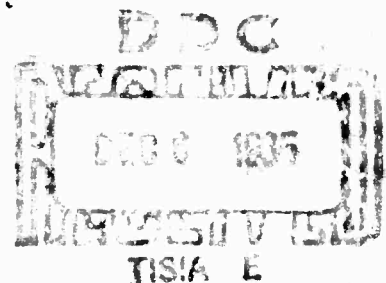
### FOR PHASED ARRAY ANTENNAS

QUARTERLY PROGRESS REPORT P-3/321

APRIL 1, 1965 TO JUNE 30, 1965

CLEARINGHOUSE FOR FEDERAL SCIENTIFIC AND TECHNICAL INFORMATION			
Hardcopy	Microfiche		
\$3.00	\$0.75	63 pp	05
ARCHIVE COPY			

*Code 1*



AD624132

**BEST  
AVAILABLE COPY**

# COLUMBIA UNIVERSITY

IN THE CITY OF NEW YORK

SCHOOL OF ENGINEERING AND APPLIED SCIENCE  
ELECTRONICS RESEARCH LABORATORIES

632 WEST 125th STREET  
NEW YORK, NEW YORK 10027

CU-13-AF-1478-ERL

July 1, 1965

## ELECTRO-OPTICAL SIGNAL PROCESSING TECHNIQUES FOR PHASED ARRAY ANTENNAS

QUARTERLY PROGRESS REPORT P-3/321

APRIL 1, 1965 TO JUNE 30, 1965

Prepared for  
Director  
Advanced Research Projects Agency  
Washington D. C. 20301  
and  
Director of Physical Sciences  
Air Force Office of Scientific Research  
Office of Aerospace Research  
U. S. Air Force  
Washington, D. C. 20333  
Contract No. AF 49 (638)-1478  
ARPA Order No. 279



ABSTRACT

The research program for the development of electro-optical signal processing techniques applicable to phased array antenna systems is continued.

A brief analysis of the planar array processor formed by combining the "spatially multiplexed" and "time-delay multiplexed" linear array processor techniques is presented. A description of the experimental system and the results obtained when processing signals simulating the output from a uniformly weighted planar array of 576 elements is included. It is shown that the output response is very nearly ideal for signals on and off the boresight axis.

The experimental results obtained with a spatial filter system at the laser output beam, and the frequency response of the multiple transducer are also included.

The theory and techniques developed for aperture weighting in the time-delay multiplex signal simulator are discussed.

AUTHORIZATION

The research described in this report was performed at the Electronics Research Laboratories of the School of Engineering and Applied Science of Columbia University. This report was prepared by A. Aimette and N. Wyman.

This project is directed by the Advanced Research Projects Agency of the Department of Defense and is administered by the Air Force Office of Scientific Research under Contract AF 49(638)-1478.

Submitted by:

L. Lambert  
Laboratory Supervisor

Approved by:

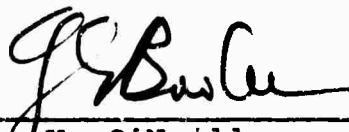
  
For L. H. O'Neill  
Associate Dean  
Director

TABLE OF CONTENTS

	<u>Title</u>	<u>Page</u>
	ABSTRACT	ii
I.	INTRODUCTION AND SUMMARY OF RESULTS	1
II.	THE ELECTRO-OPTICAL PROCESSING FOR PLANAR ARRAY ANTENNAS	6
	A. THE THEORETICAL RESPONSE OF THE PLANAR ARRAY PROCESSOR	6
	B. THE PLANAR ARRAY PROCESSOR EXPERIMENTAL SYSTEM	11
	C. THE EXPERIMENTAL PROGRAM RESULTS	17
	1. The Zero Order System Response	17
	2. The Planar Array Processor Response	20
	3. The Multiple Transducer Frequency Response	23
	4. The Spatial Filtering Experimental Results	30
III.	TIME MULTIPLEX SIMULATOR WITH APERTURE WEIGHTING	36
	A. AMPLITUDE WEIGHTING - TIME-DELAY MULTI- PLEX SIGNAL SIMULATOR	36
	B. THE IMPLEMENTATION OF AMPLITUDE WEIGHTING FOR THE TIME DELAY MULTIPLEX SIGNAL SIMULATOR	42
	1. Weighting of the Time Multiplexed Signal	42
	2. Sampling of Spectrum	46
IV.	REFERENCES	54

LIST OF FIGURES

<u>Fig. No.</u>	<u>Title</u>	<u>Page</u>
1	Schematic Diagram - Planar Antenna Array Processor System	7
2	Experimental Planar Array Electro-Optical Signal Processor	12
3	Block Diagram of Signal Simulator to Generate a Time-Multiplexed Waveform	14
4	Block Diagram for 24-Channel Spatially Multiplexed Signal Simulator and Transducer Drivers	15
5	Zero Order Fringe Light Intensity Distribution Along $\theta$ -Axis ( $y'$ -Axis)	18
6	Zero Order Fringe Light Intensity Distribution Along $\psi$ -Axis ( $x'$ -Axis)	19
7	Planar Array Processor Measured Output Response, $\theta$ -Axis for Simulated Signal on Boresight ( $\theta_o \equiv 0, \psi_o \equiv 0$ )	21
8	Planar Array Processor Measured Output Response, $\psi$ -Axis for Simulated Signal on Boresight ( $\theta_o \equiv 0, \psi_o \equiv 0$ )	22
9	Planar Array Processor Measured Output Response, $\theta$ -Axis for Simulated Signal at ( $\theta_o = 0, \psi_o = 19.5^\circ$ ) Off Boresight	24
10	Planar Array Processor Measured Output Response, $\psi$ -Axis for Simulated Signal at ( $\theta_o = 0, \psi_o = -19.5^\circ$ ) Off Boresight	25
11	Planar Array Processor Measured Output Response, $\theta$ -Axis for Simulated Signal at ( $\theta_o = -19.5^\circ, \psi_o = -19.5^\circ$ ) Off Boresight	26

LIST OF FIGURES (CONT'D.)

<u>Fig. No.</u>	<u>Title</u>	<u>Page</u>
12	Planar Array Processor Measured Output Response, $\psi$ -Axis for Simulated Signal at $(\theta_0 = -19.5^\circ, \psi_0 = -19.5^\circ)$ Off Bore-sight	27
13	Planar Array Processor Measured Output Response, $\theta$ -Axis for Simulated Signal at $(\theta_0 = -19.5^\circ, \psi_0 = +41.6^\circ)$ Off Bore-sight	28
14	Planar Array Processor Measured Output Response, $\psi$ -Axis for Simulated Signal at $(\theta_0 = -19.5^\circ, \psi_0 = +41.6^\circ)$ Off Bore-sight	29
15	Experimental Frequency Response of Multiple Channel Transducers	31
16	The Measured Light Intensity Distribution in the Collimated Region of the Optical System	32
17	Zero Order Light Intensity Distribution in Output Focal Plane (Without Spatial Filter)	33
18	The Measured Light Intensity Distribution in the Collimated Region of the Optical System (with Spatial Filtering)	34
19	Zero Order Light Intensity in Output Focal Plane with Spatial Filter	35
20	Variation of 2nd Sidelobe of Output Focal Plane Light Distribution as a Function of Aperture Shift	41
21	First Sidelobe Level Increase as Function of $T_2/T_1$	43
22	Block Diagram of Signal Simulator to Generate a Time-Multiplexed Waveform	44



LIST OF FIGURES (CONT'D.)

<u>Fig. No.</u>	<u>Title</u>	<u>Page</u>
23	Time-Multiplex Signal Weighting Block Diagram and Waveforms	45
24	Modulation Shaper and Amplitude Modulator	47
25	Spectrum Sampling Block Diagram and Wave- forms	48
26	Logarithmic Amplifier	50
27	Sampling System	52

I. INTRODUCTION AND SUMMARY OF RESULTS

The objective of this research program is the application of electro-optical signal processing techniques to planar array antennas. Both theoretical and experimental investigations have been performed at these Laboratories to demonstrate the engineering feasibility for such an application. Previous reports of this program<sup>1-8</sup> contain the results of these investigations in detail. A brief resume of the past results of this research program follows.

Two techniques have been developed for processing the output signals of linear array antennas: the spatially multiplexed technique and the time-delay multiplexed technique. Each of these methods, when utilized in conjunction with a coherent optical system, is capable of processing the output signals from a linear array antenna. When both of these techniques are used simultaneously, the output signals from planar array antennas can be processed.

In the spatially multiplexed system the signal output from each element in a linear array is the input to separate channels in an ultrasonic light modulator. The channel transducers are positioned to generate parallel acoustic beams which propagate perpendicularly to the direction of light passing through the cell. Since the input signal to each channel possesses a phase delay proportional to the angle of signal arrival at the array,  $\theta_0$ , the light emanating from the cell is modulated with this same phase information. The integrating lens forms the far-field pattern of this modulated light in the output focal plan, and the position of the main

<sup>1</sup> For numbered references, see Sec.IV.

lobe is displaced in direct proportion to the angle of interest  $\theta_0$ . Note that all angles of interest,  $|\theta_0| \leq 90$  deg, are processed continuously and simultaneously. When the antenna is illuminated by the return signals from a multiplicity of targets, each target will appear as a separate and unambiguous peak of light.

A 24-channel spatially multiplexed system has been constructed and tested. The system employs a multiple channel transducer operating at 20 mc with a bandwidth of 1.25 mc. Each channel is provided with a separate, 5-mc bandwidth, variable phase, variable gain driver-amplifier to permit the simulation of various signal arrival angles and antenna aperture distributions.

The experimental results obtained with this system indicate that a stable, very nearly ideal output response was obtained for simulated targets at angles in the range of  $\pm 90$  deg for a uniform antenna distribution. The resolution, sidelobe level, and main-lobe position were identical to the output as predicted by the theoretical model for the array. When an output signal from an array with a Hanning-type aperture distribution was simulated, the system resolution and peak position measured were as predicted by theory; the measured sidelobe level, however, was limited by lens errors to 28 db below the main light peak. Further investigation has shown this sidelobe level is consonant with lenses corrected to a  $1/8$  wavelength.

The time-delay multiplex technique utilizes one ultrasonic light modulator channel for a linear array of elements. The output signal from each element of the array is delayed and summed with the output signal from the other elements to form a continuous pulse train input signal to the channel. The

relative phase of each pulse in the ensemble is proportional to the signal arrival angle at the linear array  $\psi_0$ . As this pulse train propagates through the water medium of the light modulator cell, the light passing through the acoustic beam is phase modulated according to this target angle phase information. The field pattern main lobe displacement corresponding to this phase modulation is orthogonal to the spatially multiplexed displacement. By measuring both displacements of the main lobe peak(s) the angular location of the target(s) which illuminated the planar antenna aperture may be ascertained.

A time delay multiplexed signal simulator was designed and constructed. The simulator generates a continuous train of 20-mc carrier, 0.8- $\mu$ sec pulses by sequentially gating the output of 12 variable phase channels. To provide a capability of simulating the output of an antenna with more than twelve elements the angles simulated were restricted to those for which the total phase delay of 12 channels was an integral number of carrier cycles. For these angles the phase distribution between each group of 12 pulses is continuous and the number of elements which may be processed is limited by the length of the optical aperture. Aperture lengths of 28.8 and 57.6 mm provided a capability of processing 24 and 48 elements, respectively. The output of the signal simulator was the input to a single channel ultrasonic light modulator; a 20-mc, 1.4-mc bandwidth unmatched transducer was employed to generate the acoustic beam.

The beamwidth and sidelobe response obtained with this experimental system, when processing the simulated output from uniformly weighted antenna arrays of 24 and 48 elements (for angles  $|\psi_0| \leq 90$  deg), were identical to the inherent theoretical capabilities of the array.

Therefore, the capability for processing the output from linear array antennas utilizing the spatial and the time-delay multiplex techniques has been demonstrated. To process the output of a planar array both methods are employed simultaneously in a single optical configuration as follows:

The output signal from the time-delay multiplex signal simulator is the input to each channel of the spatially multiplexed system. The two-dimensional phase information of the target return signal impinging upon the elements of the planar array is translated into a two-dimensional spatial phase distribution within the light modulator. The phase distribution along the orthogonal axes of the plane perpendicular to the direction of light propagation in the light modulator is proportional to the two angles  $(\theta_o, \psi_o)$  which define the target location in space. The far field intensity distribution of the modulated light output is, therefore, the direct optical analogue of the far-field pattern of the planar antenna array. A measurement of the position(s) of the peak(s) in the output focal plane, determines the angular location of the target(s)  $(\theta_o, \psi_o)$  which contributed to the antenna aperture illumination.

During this past report period the time-delay multiplex signal simulator and the spatially multiplexed system were combined. The 24-channel spatially multiplexed system and time-delay multiplex aperture length of 28.8 mm provided the capability for processing the simulated signals from a uniformly weighted planar array of 576 elements. The system output response along the orthogonal output focal plane coordinates was identical to the response of the systems operating separately. The beamwidth, sidelobe response, and main lobe displacement measurements indicate that the electro-optical processor output for the planar array is very nearly ideal for

targets at various location angle combinations,  $(\theta_o, \psi_o)$ ,  $|\theta_o|$  and  $|\psi_o| \leq 90$  deg.

The spectrum of the time-delay multiplexed signal simulator was obtained with a conventional electronic spectrum analyzer and compared with the electro-optical system response. Since the light intensity distribution is directly proportional to the power spectrum of the input signal, the electronic spectrum and the system response should be essentially identical; the data obtained verified this prediction.

A spatial filtering technique was implemented to remove the small amplitude perturbations in the light input to the system. The results obtained show that this technique has eliminated the sidelobe variations in the output focal plane intensity distribution.

A technique for amplitude weighting the time-delay multiplex signal with a synchronously generated modulation waveform was also developed. Since the light intensity distribution in the output focal plane is time-varying at the modulation frequency, a system to sample the photomultiplier output voltage was designed and constructed. During this next program period the system response to weighted aperture distribution in both dimensions will be measured.

## II. THE ELECTRO-OPTICAL PROCESSING FOR PLANAR ARRAY ANTENNAS

### A. THE THEORETICAL RESPONSE OF THE PLANAR ARRAY PROCESSOR

Fig. 1 schematically depicts the operational relationships between the planar array and the optical processor.

The planar array lies in the  $x,y$  plane and consists of a matrix of  $M \times N$  elements in rows and columns spaced  $d$  units apart. A plane wave signal return, of duration  $T$ , impinges upon the array from a target located at range  $R$ , and at angles  $(\theta_0, \psi_0)$  with respect to the column and row axes of the array. As the wave traverses the plane of the array, a signal output appears at the terminal of each element.

Consider the signal appearing at the linear array formed by the  $M$  elements in the  $n$ th column. The signal output from the  $(m,n)$  element may be written as

$$V_{n,m}(t) = P_T(t - m\tau_1 - n\tau_2) \sin 2\pi \left[ f_R(t - m\tau_1 - n\tau_2) \right] \quad (1)$$

where

$$t = t' - \tau_R$$

$$\tau_R = 2R/C$$

$t'$  = time referenced to transmitter

$$f_R = f_c + f_d$$

$$f_d = 2Rf_c/C$$

$\tau_1$  = incremental delay between elements in the column

$$= \frac{d}{C} \sin \psi_0$$

$\psi_0$  = angle of signal arrival with respect to the column axis

$\tau_2$  = incremental delay between columns

$$= \frac{d}{C} \sin \theta_0$$

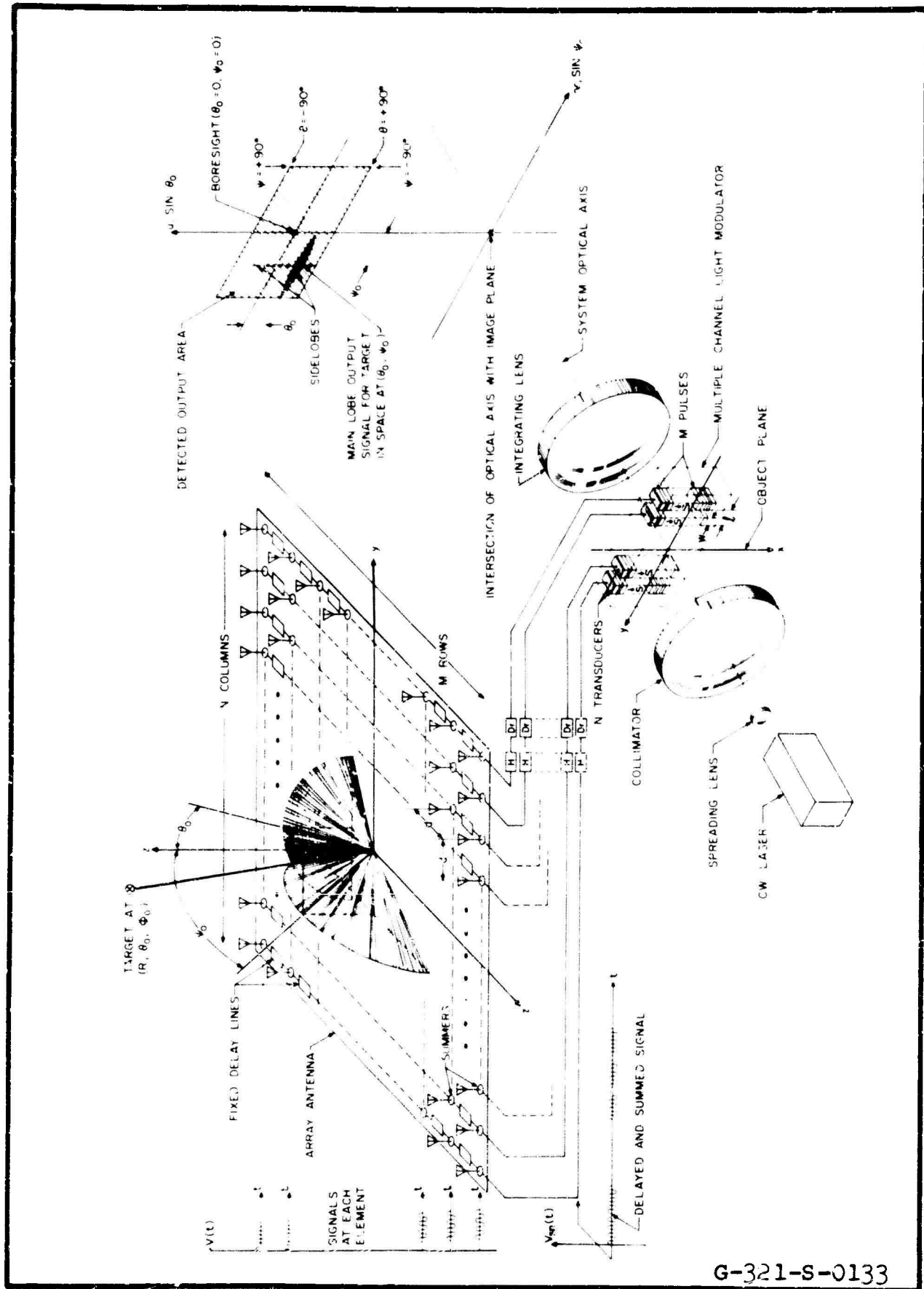


Fig. 1 Schematic Diagram - Planar Antenna Array Processor System



$\theta_0$  = angle of signal arrival with respect to the row axis and the function  $P_T(t)$  is defined as

$$P_D(z) \equiv \begin{cases} 1, & |z| \leq D/2 \\ 0, & |z| > D/2 \end{cases}$$

To process the output from each  $n$ th column of elements, the ensemble of array element signals  $V_{nm}(t)$  from that column is "time multiplexed" by delaying the signals from adjacent elements with a constant incremental delay  $T_D$  chosen so that

$$T_D \geq T + |\tau_1|_{\max} \quad (2)$$

and summing the  $M$  signals to form a continuous pulse train of duration  $MT_s$  where

$$T_s \equiv T_D + \tau$$

The pulse train is heterodyned to the light modulator transducer frequency  $f_0$  and may be written as

$$V_n(t) = \sum_{m = -\left(\frac{M-1}{2}\right)}^{m = \left(\frac{M-1}{2}\right)} P_T(t - mT_s - n\tau_2) \sin 2\pi \left[ f_i(t - mT_s) - n\alpha_2 - m\alpha_1 \right] \quad (3)$$

where

$$f_i = f_0 + f_d$$

$$\alpha_1 = \frac{d}{\lambda_c} \sin \psi_0$$

$$\lambda_c = \text{carrier wavelength}$$

$$\alpha_2 = \frac{d}{\lambda_c} \sin \theta_0$$

The time multiplexed output signals from the  $N$  columns of the array Eq. (3) are now "spatially multiplexed" in the multiple channel light modulator. The output signal from the  $n^{\text{th}}$  column of the array is the input signal to the  $n^{\text{th}}$  channel of the light modulator. Each transducer in the light modulator converts the electrical input signal from each array column to an acoustic beam propagating at the sonic velocity  $S$  in the  $x$  direction of the object plane. Since the time-multiplexed signals consist of  $M$  rf pulses spaced  $T_s$  apart, the length of the ultrasonic beam, at the instant it fills the aperture is  $D \equiv SMT_s$  meters. The width of the aperture along  $y$  is  $L \equiv Nl$ , since there are  $N$  transducers each  $w$  wide and spaced  $l$  apart.

Consider the relative phase distribution in the light modulator at the instant when all the signals from the array are in the  $L \times D$  aperture. Each ultrasonic beam consists of  $M$  pulses along the  $x$  coordinate of the image plane; the phase difference between each pulse is proportional to the target location angle with respect to the corresponding column of elements in the planar array,  $\psi_o$ . The phase difference between each ultrasonic channel (along the  $y$  axis of the image plane) is proportional to the angle of signal arrival with respect to the row of elements in the planar array,  $\theta_o$ . The two dimensional phase information across the aperture of the array, corresponding to the two target location angles,  $(\theta_o, \psi_o)$  has been converted into a two dimensional acoustic phase distribution in the image plane of the optical system.

The plane, coherent light beam, formed by the laser, the spreading lens, and the collimating lens is phase modulated as it passes through the acoustic beams of the multiple channel light modulator. The light intensity distribution in the output focal plane of the integrating lens is the optical analogue of the planar array illumination. The location of the first

order main peak of light, in terms of the  $(u,v)$  coordinates, is directly proportional to the angular location of the target. It may be shown that the light intensity distribution in the vicinity of the light peak of interest, corresponding to an input signal of the form given in Eq. (3), is given by

$$I(u,v) = I(u) I(v) \quad (4)$$

where

$$I(u) \equiv \left[ \text{sinc } T(us - f_i) \right]^2 \cdot \left[ \frac{\sin \pi M(us T_D - \alpha_1)}{\sin \pi(us T_D - \alpha_1)} \right]^2 \quad (5)$$

$$I(v) \equiv \left[ \text{sinc } wv \right]^2 \cdot \left[ \frac{\sin \pi N(v\ell + \alpha_2)}{N \sin \pi(v\ell + \alpha_2)} \right]^2 \quad (6)$$

and

$$\text{sinc } Z \equiv \frac{\sin \pi Z}{\pi Z},$$

$$\alpha_1 = \frac{d}{\lambda_c} \sin \psi_o, \quad |\psi_o| \leq 90^\circ, \quad (7)$$

$$\alpha_2 = \frac{d}{\lambda_c} \sin \theta_o, \quad |\theta_o| \leq 90^\circ.$$

Equations 5 and 6 are the theoretical system response of the time-multiplexed and spatially multiplexed systems respectively. The normalized output focal plane coordinates  $(u,v)$  are related to the physical plane  $(x',y')$  coordinates by the relations

$$x' = uF\lambda_L$$

$$y' = vF\lambda_L$$

$$F \equiv \text{focal length of integrating lens}$$

$$\lambda_L \equiv \text{light wave length}$$

(8)

The theoretical system response given by Eqs. 4, 5, and 6 will be compared with simulated signals and the experimental results in the next sections.

#### B. THE PLANAR ARRAY PROCESSOR EXPERIMENTAL SYSTEM

The experimental system developed to test the engineering feasibility of the electro-optical processing techniques is shown in Fig. 2.

The coherent optical system consists of a He-Ne cw gas laser operating at  $6328 \text{ \AA}$  with total power output of 4 milliwatts. The 5-mm laser beam is diverged with a 10 mm focal length microscope objective lens and is spatially filtered with a 20-micron pinhole placed at the focal point of the objective. The expanded and filtered light beam is recollimated by the F6 air spaced doublet collimation lens. A  $72 \times 28.8 \text{ mm}$  aperture-stop limits the input beam and defines the aperture for the system. A precision ruled channel separator mask, which forms one wall of the light modulator cell, divides the input beam into 24,  $1.5 \times 28.8 \text{ mm}$  beams, one for each channel of the light modulator. The multiple transducer is a 20 mc center frequency X-cut synthetic quartz plate with 24,  $1.5 \times 8.6 \text{ mm}$  gold strips, spaced 3 mm apart ( $w = 1.5 \text{ mm}$ ,  $l = 3 \text{ mm}$ ). The light modulator cell is filled with ultra-pure distilled water, and an acoustic absorber prevents reflection of the acoustic beams.

The modulated light beams from the cell are focused by another F6, 1-meter focal length, air spaced doublet lens. The light intensity distribution in the output focal plane is scanned with a  $1 \times 40 \text{ micron}$  slit mounted on a precision slide mechanism. The slit transport mount and drive assembly can be rotated  $90^\circ$ , providing a capability for scanning along either of the orthogonal axes of the output focal plane.

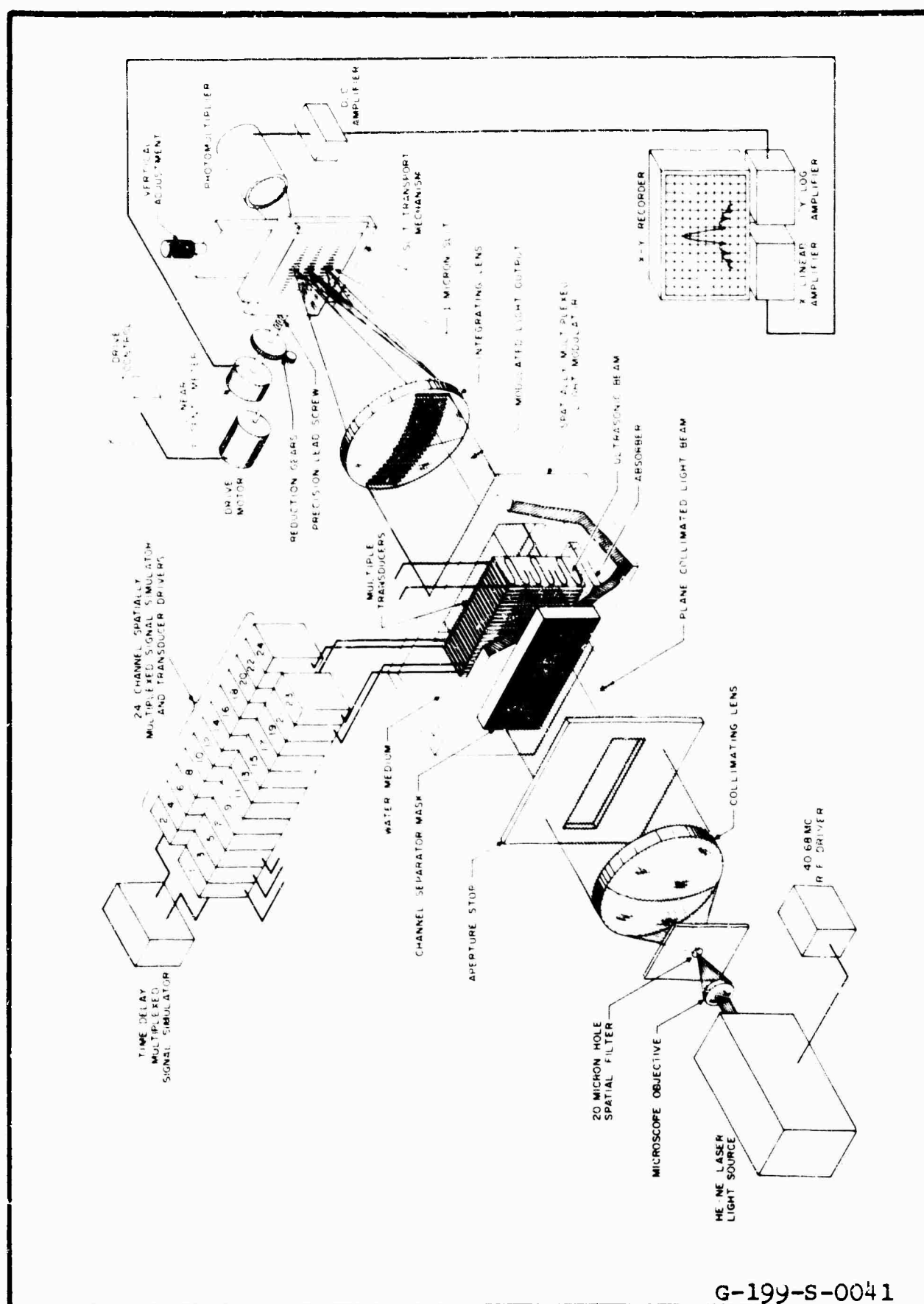


Fig. 2 Experimental Planar Array Electro-Optical Signal Processor

The light output from the slit is detected by a linear, 35 db dynamic range, photomultiplier tube. The voltage output from the photomultiplier is inverted and amplified by a DC amplifier to match the input impedance of the "y" channel log amplifier of the "x,y" recorder. A precision, infinite resolution potentiometer on the slide transport system generates the analogue position voltage for the "x" channel of the recorder. The recorder, therefore, displays the fine structure of the output focal plane light intensity distribution directly. Typical display scales are 5 db/inch and 25  $\mu$ /inch.

The planar array signal simulator is formed by combining the time-delay and the spatially multiplexed simulators discussed previously.<sup>4-8</sup> The block diagrams for the two systems are shown in Figs. 3 and 4.

The time-delay multiplexed signal simulator (Fig. 3) generates a continuous train of 20 mc carrier pulses whose relative phase can be preset to simulate various angles  $\psi_0$ . A 1.25 mc master oscillator simultaneously triggers a digital clock and a frequency multiplier. The digital clock generates pulses of period 0.8  $\mu$ sec, corresponding to the pulse width T. The frequency multiplier output is the 20-mc carrier which is multiplexed to 12 channels. Each channel contains a delay line and a transmission gate. A given target angle  $|\psi_0| \leq 90^\circ$  is simulated by delaying the carrier signal in channel M relative to the carrier in the  $M \pm 1$  channel by an amount  $|\pi \sin \psi_0|$ . The delayed carrier then appears as the input to the transmission gate. The transmission gates are sequentially turned on for 0.8  $\mu$ sec by the ring counter, driven by the digital clock output. When the gate is on, the phased carrier is passed to the summer-amplifier and summed with all the other gate output signals.

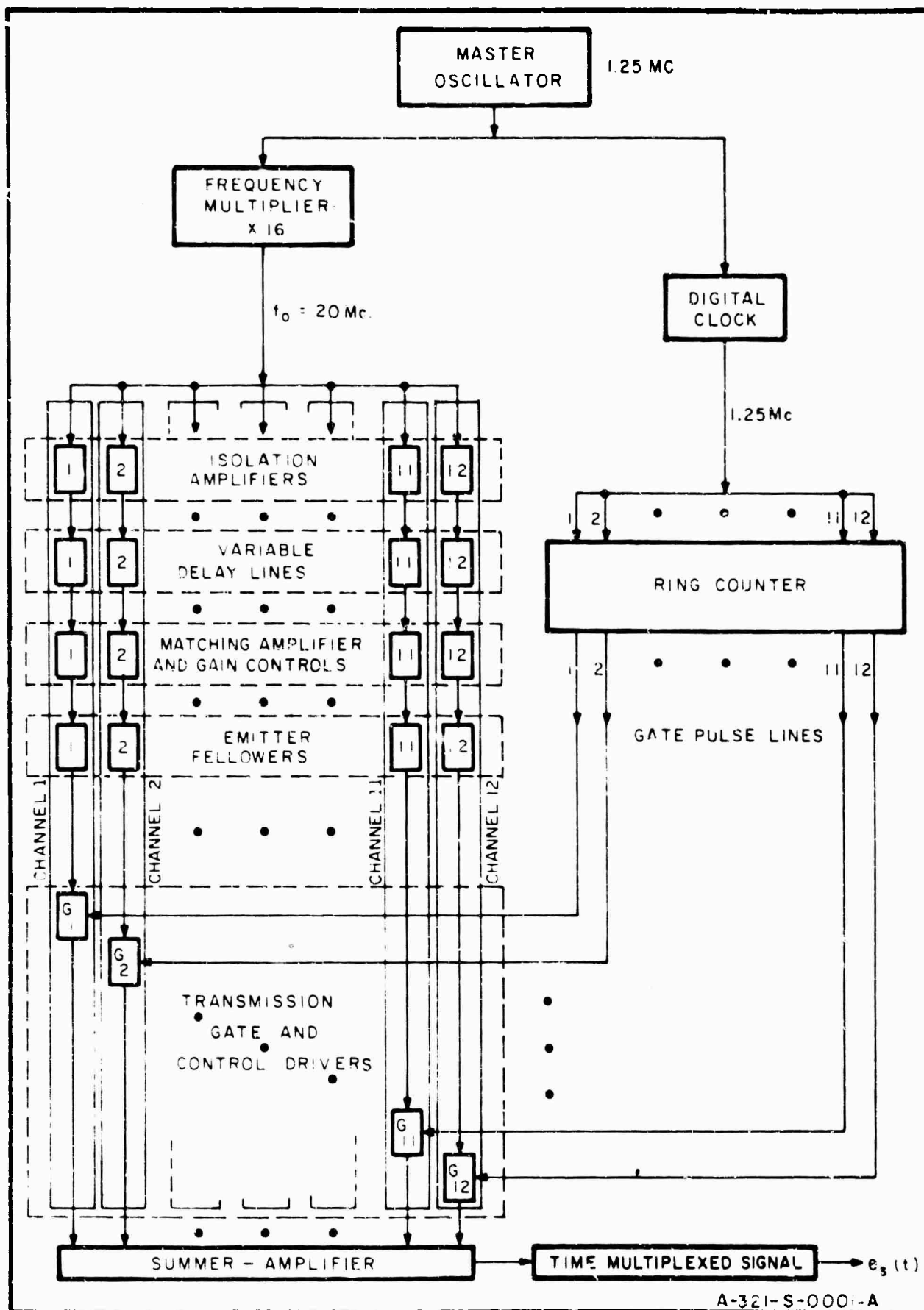


Fig. 3 Block Diagram of Signal Simulator to Generate a Time-Multiplexed Waveform

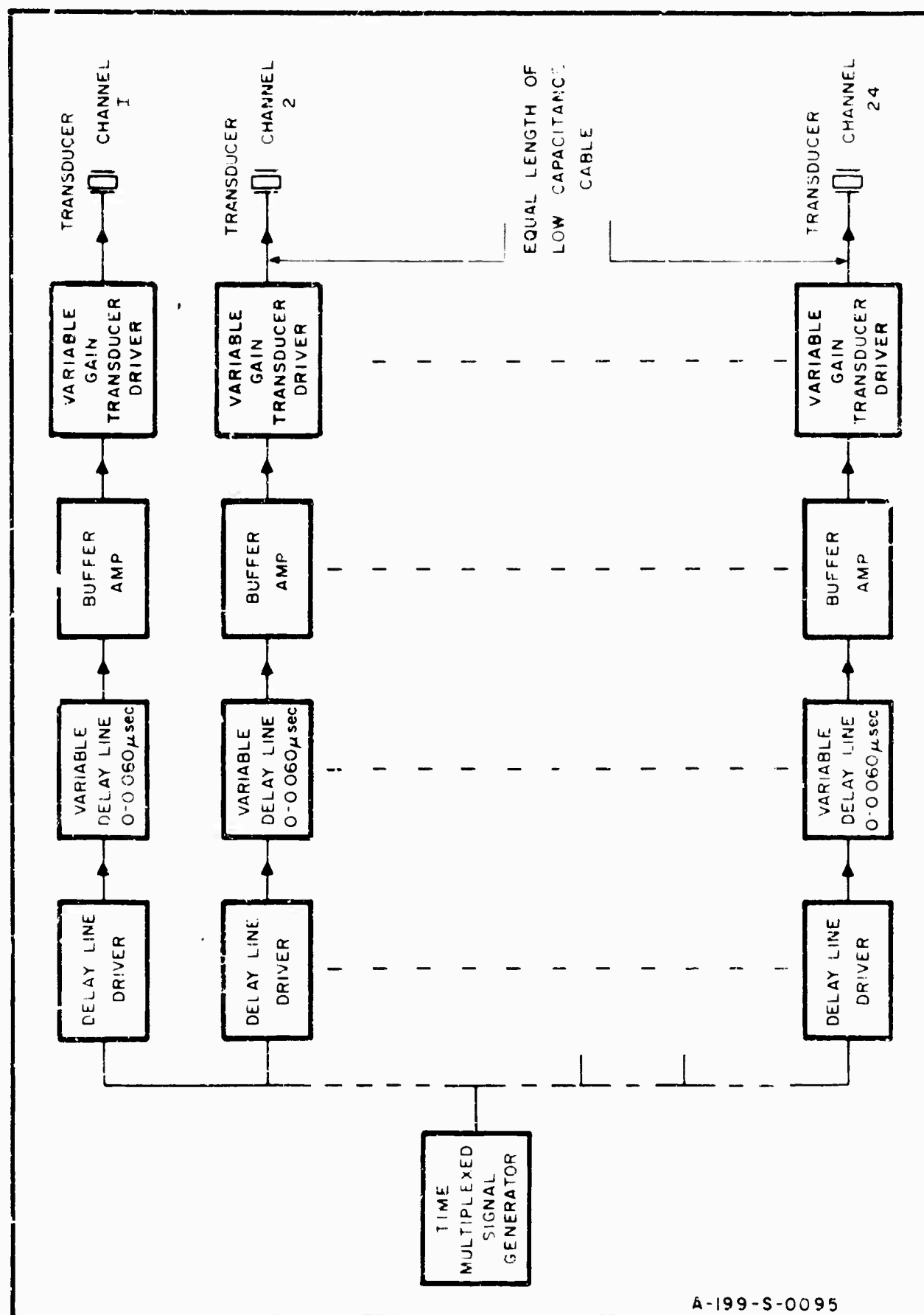


Fig. 4 Block Diagram for 24-Channel Spatially Multiplexed Signal Simulator and Transducer Drivers



The output from the simulator is therefore a 100% duty-cycle, continuous train of 12, 0.8  $\mu$ sec pulsed 20-mc carriers of period 9.6  $\mu$ sec. If the angles simulated are restricted to those for which the total incremental 12-pulse phase delay is a multiple of the carrier period,  $1/f_0$ , the number of element output signals which may be simulated is determined by the length of the optical system aperture. For an aperture length of 28.8 mm the optical system can process 24 elements since each pulse of 0.8  $\mu$ sec occupies a length of 1.2 mm in the aperture.

The output signal from the time multiplex generator is the input to each of the 24 channels of the spatially multiplexed system. Each channel has a 5-mc bandwidth centered at 20 mc with a (0 - 0.060)  $\mu$ sec delay line and a (0 - 10) variable gain amplifier. The relative phase between channels is set to simulate the second angle of arrival  $\theta_0$ . A weighted aperture distribution can be simulated by adjusting the relative gain of each channel driver. The output stage of each channel is matched to the input impedance of the transducer.

As derived previously<sup>8</sup> the theoretical response in the region of interest of the output focal plane for the experimental system as described above can be written as

$$I(u,v) = I(u) I(v) \quad (9)$$

$$I(u) \doteq \text{sinc}^2 N(uTS - Tf_0 + \alpha_1) + \left( \frac{\alpha_1 A_{-1}}{\alpha_1 + 1} \right)^2 \text{sinc}^2 N(uTS - Tf_0 + \alpha_1 + 1) + \left( \frac{\alpha_1 A_{+1}}{\alpha_1 - 1} \right)^2 \text{sinc}^2 N(uTS - Tf_0 + \alpha_1 - 1) \quad (10)$$

$$I(v) = \text{sinc}^2 wv \cdot \left[ \frac{\sin \pi N(vl + \alpha_2)}{\sin \pi(vl + \alpha_2)} \right]^2 \quad (11)$$

Comparing Eqs. 9 and 10 with Eqs. 5 and 6 shows that the spatially multiplexed simulated response and the theoretical response are identical. However, the time multiplexed simulated signal response (Eqs. 5 and 10) are different. Equation 5 was written for the instant of time when the signal fills the light modulator aperture. The signal simulator output, however, is continuous in time and propagates through the aperture at the sonic velocity  $S$ . The output focal plane light intensity distribution is therefore a time varying signal and Equation 5 is modified to reflect this dependence. The constants  $A_{\pm 1}$  are the weighting factors of the transducer frequency response and are determined experimentally for each angle,  $\psi_0$ , simulated. Equations 10 and 11 will now be utilized to evaluate the results obtained with the experimental system.

### C. THE EXPERIMENTAL PROGRAM RESULTS

#### 1. The Zero Order System Response

The standard of comparison for the experimental results is the output focal plane light intensity distribution (the zero order fringe) of the undiffracted light passing through the input aperture of the optical system. Figures 5 and 6 show this light intensity distribution.

Figure 5 shows the light intensity distribution along the  $\theta$  or  $y'$  axis and the scales for both physical distance and the equivalent angular units are shown. The theoretical sidelobe level, computed from Eq. 11, is indicated. The inset is a magnified photograph of the light intensity distribution as it is seen in the output focal plane. The relative light intensity of the distribution is plotted in db units on the vertical scale.

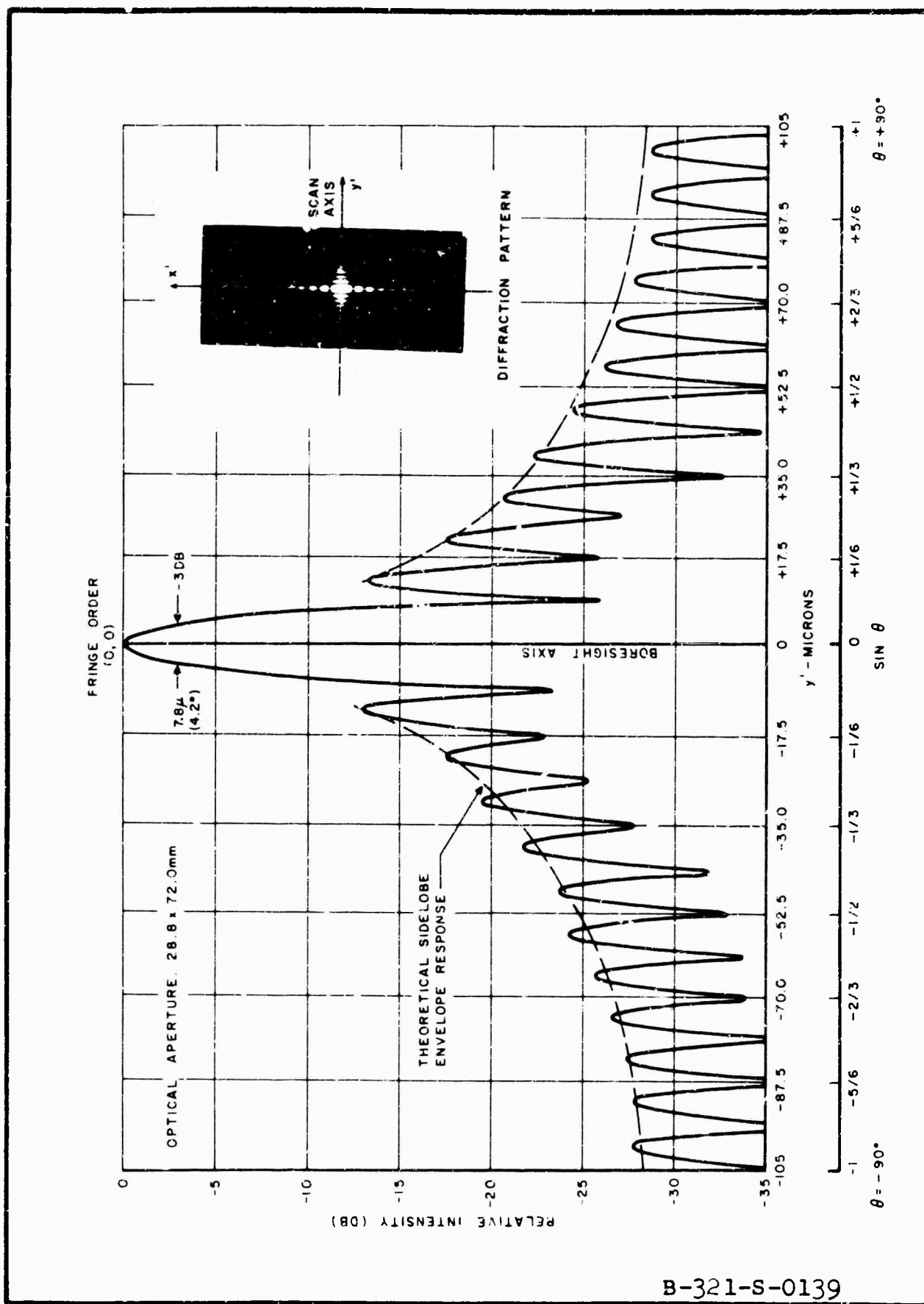


Fig. 5 Zero Order Fringe Light Intensity Distribution Along  $\theta$ -Axis ( $y'$ -Axis)

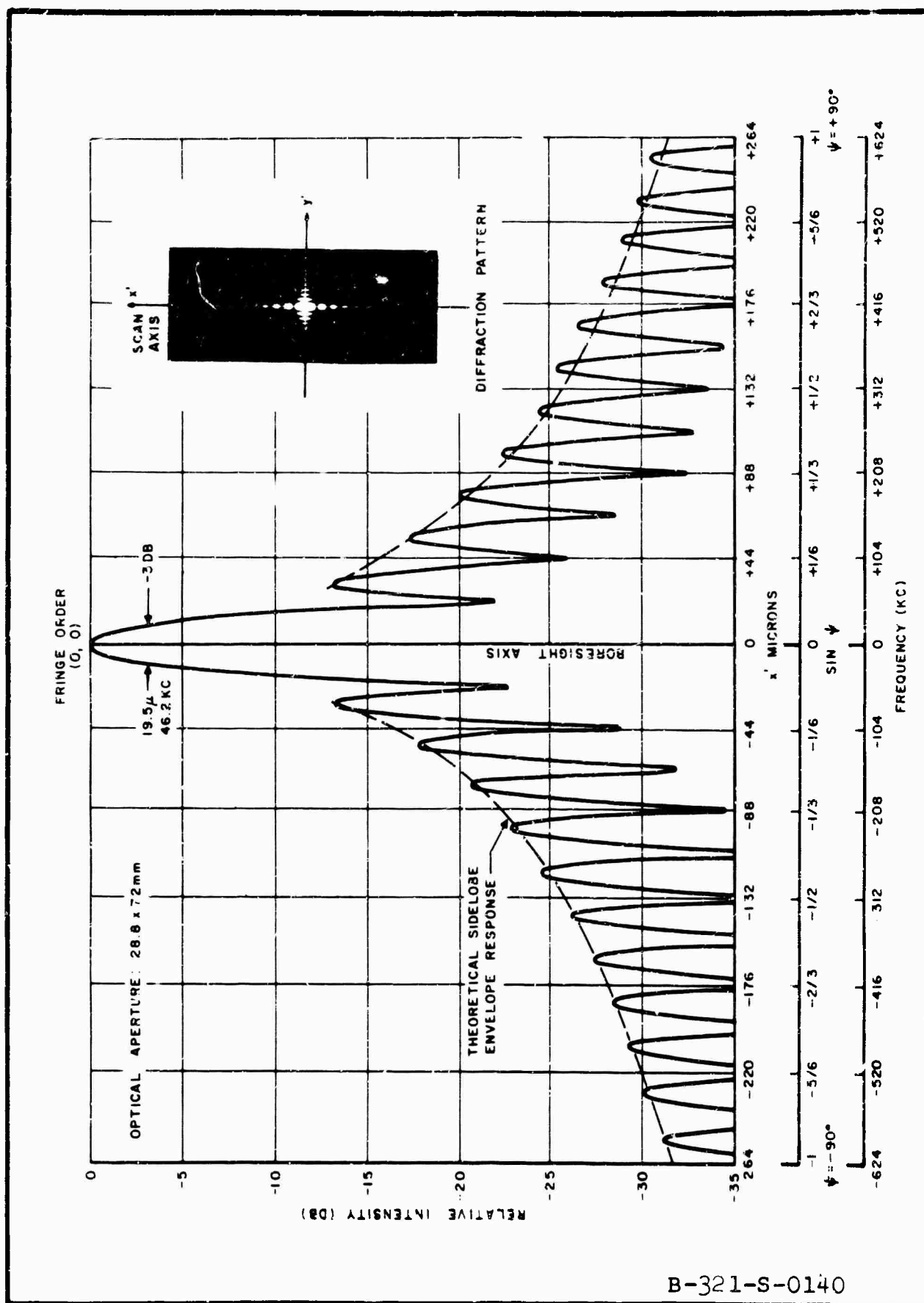


Fig. 6 Zero Order Fringe Light Intensity Distribution Along  $\psi$ -Axis ( $x'$ -Axis)

Figure 6 shows the corresponding light intensity distribution along the  $\psi$  or  $x'$  axis. The horizontal scale for this plot includes the units of frequency since physical distance along this coordinate is also proportional to the light modulator frequency according to the relation

$$x' = F\lambda_s f / \lambda \quad (12)$$

where

$F \equiv$  focal length of the integration lens

$\lambda_L =$  light wavelength

$f =$  frequency in cycles/seconds of the light modulator

$s =$  velocity of acoustic propagation

From these two figures it may be seen that the light intensity distribution is very nearly ideal. The envelope response, the half-power bandwidth, and the fine structure of the distribution are all very close to theoretically predicted values.

## 2. The Planar Array Processor Response

Figures 7 and 8 show the measured output response of the planar array processor for a simulated signal return from a target on the boresight axis of the array. These plots show the intensity distribution of the light diffracted by the light modulator cell. The peak of the distribution is located 8.44 mm (the 20-mc point) above the zero order fringe peak on the  $x'$  axis.

Figure 7 shows the light intensity distribution on the  $\theta$  or  $y'$  axis. The inset photograph shows the actual light distribution in the plane. Figure 8 shows the distribution along the  $\psi$  or  $x'$  axis. Inset A shows the light intensity distribution and the corresponding scan axis for the

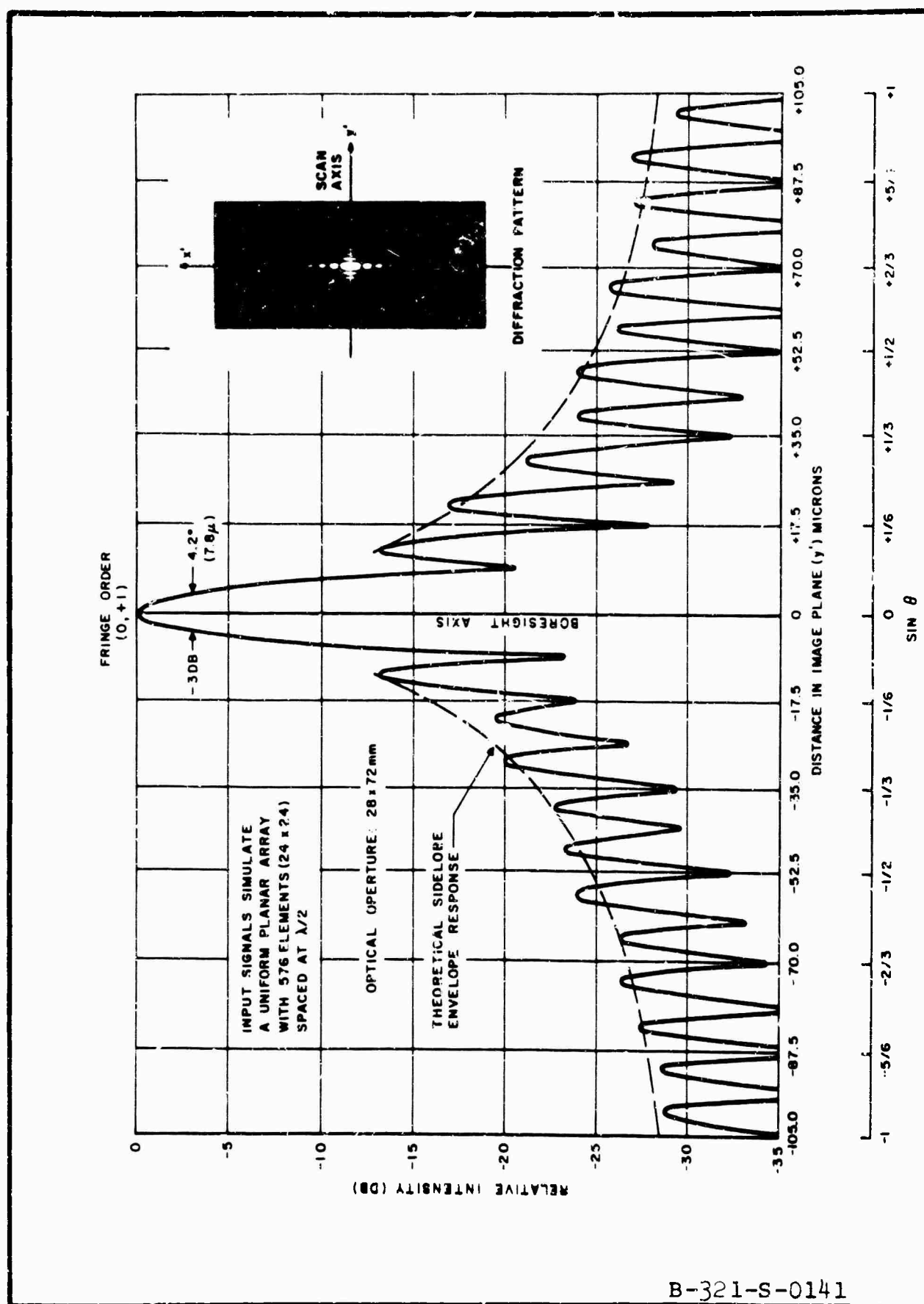


Fig. 7 Planar Array Processor Measured Output Response,  $\theta$ -Axis for Simulated Signal on Boresight ( $\theta_0 \equiv 0, \psi_0 \equiv 0$ )

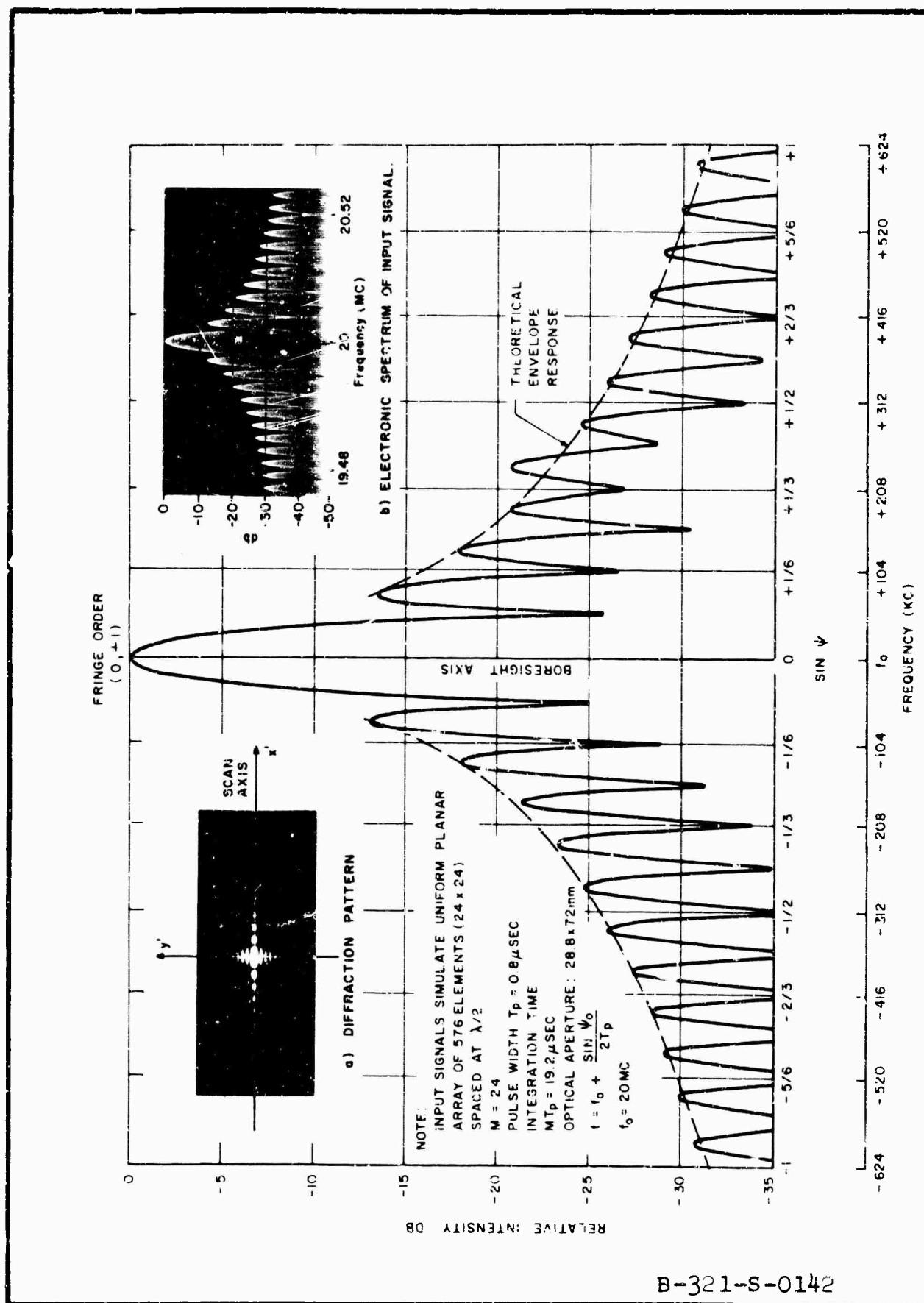


Fig. 8 Planar Array Processor Measured Output Response,  
 $\psi$ -Axis for Simulated Signal on Boresight ( $\theta_0 = 0, \psi_0 = 0$ )

graphical display. Inset B shows the electronic spectrum of the corresponding time-delay multiplex signal input. Since the light intensity distribution on the  $\psi$  axis is directly proportional to the frequency spectrum of the input signal, this technique provides a second method of evaluating the output response of the processor system.

A comparison of the results shown in Figs. 5 and 7 and Figs. 6 and 8 shows that the processor output response is essentially identical to the response of the optical system. The half power resolution width and sidelobe response is almost the same. A slight variation in the sidelobe level does exist, indicating that the processor introduces low order amplitude and/or phase errors.

Figures 9 through 14 present the output response of the processor for input signals simulating various target location angles  $[\theta_0, \psi_0]$  from a uniformly weighted planar array.

Figures 9 and 10 show the output response for a simulated signal at  $\theta_0 = 0$ ,  $\psi_0 = -19.5^\circ$  off the boresight axis.

Figures 11 and 12 show the response for  $\theta_0 = -19.5^\circ$ ,  $\psi_0 = -19.5^\circ$ .

Figures 13 and 14 show the response for  $\theta_0 = -19.5^\circ$ ,  $\psi_0 = 41.6^\circ$ .

These results are essentially identical with the boresight output response (Figs. 7 and 8) and the zero order response (Figs. 5 and 6). The theoretical envelope response shown were computed with the aid of Eqs. 10 and 11. The sidelobe variations, particularly on the  $\theta$  axis output response, indicate that small amplitude or phase variations exist but are quite small and effect only the far sidelobes in the pattern.

### 3. The Multiple Transducer Frequency Response

As mentioned previously the light intensity distribution along the  $\psi$  axis (Eq. 10) is dependent upon the transducer



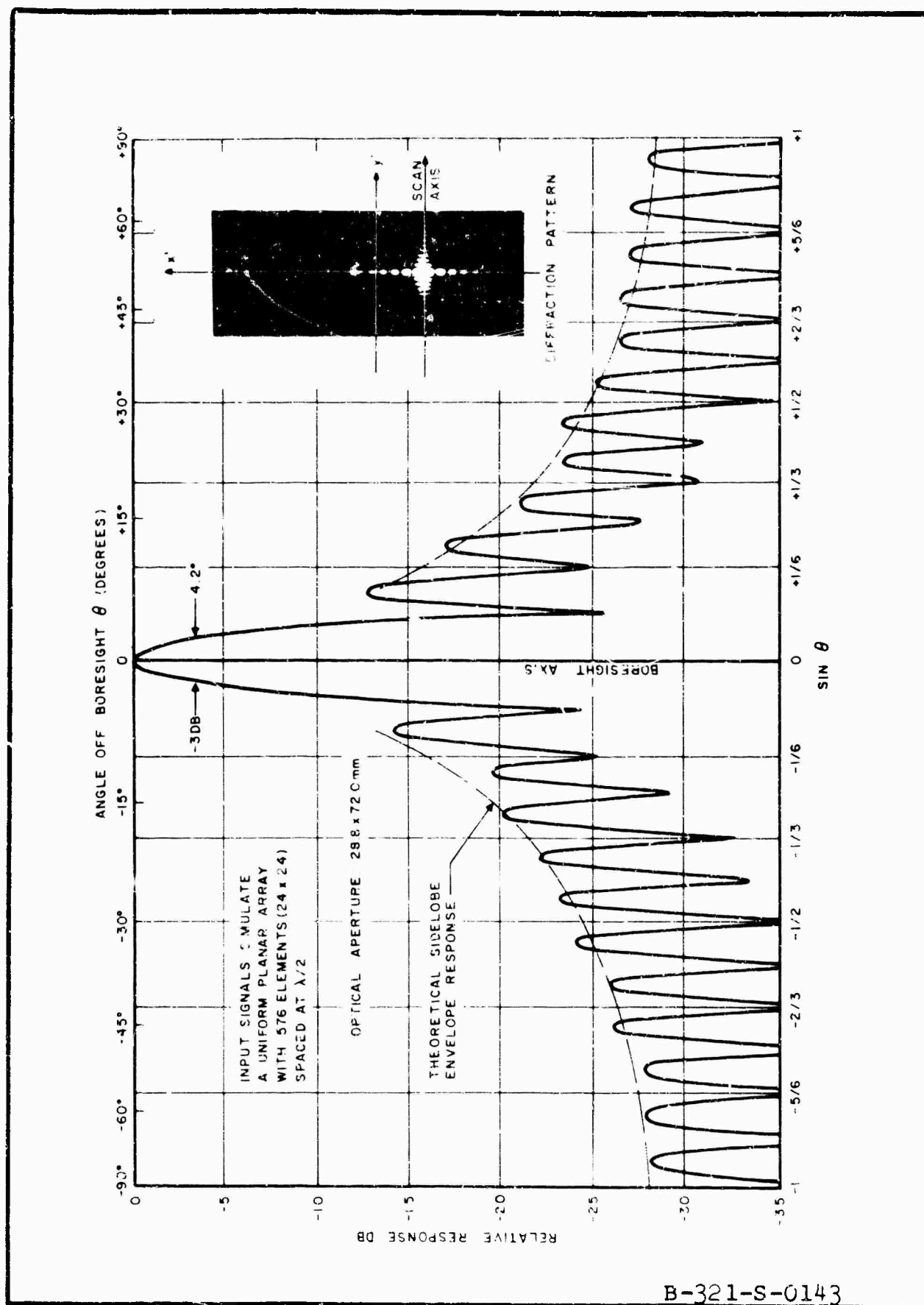


Fig. 9 Planar Array Processor Measured Output Response,  $\theta$ -Axis for Simulated Signal at  $(\theta_0 = 0, \psi_0 = 19.5^\circ)$  Off Boresight

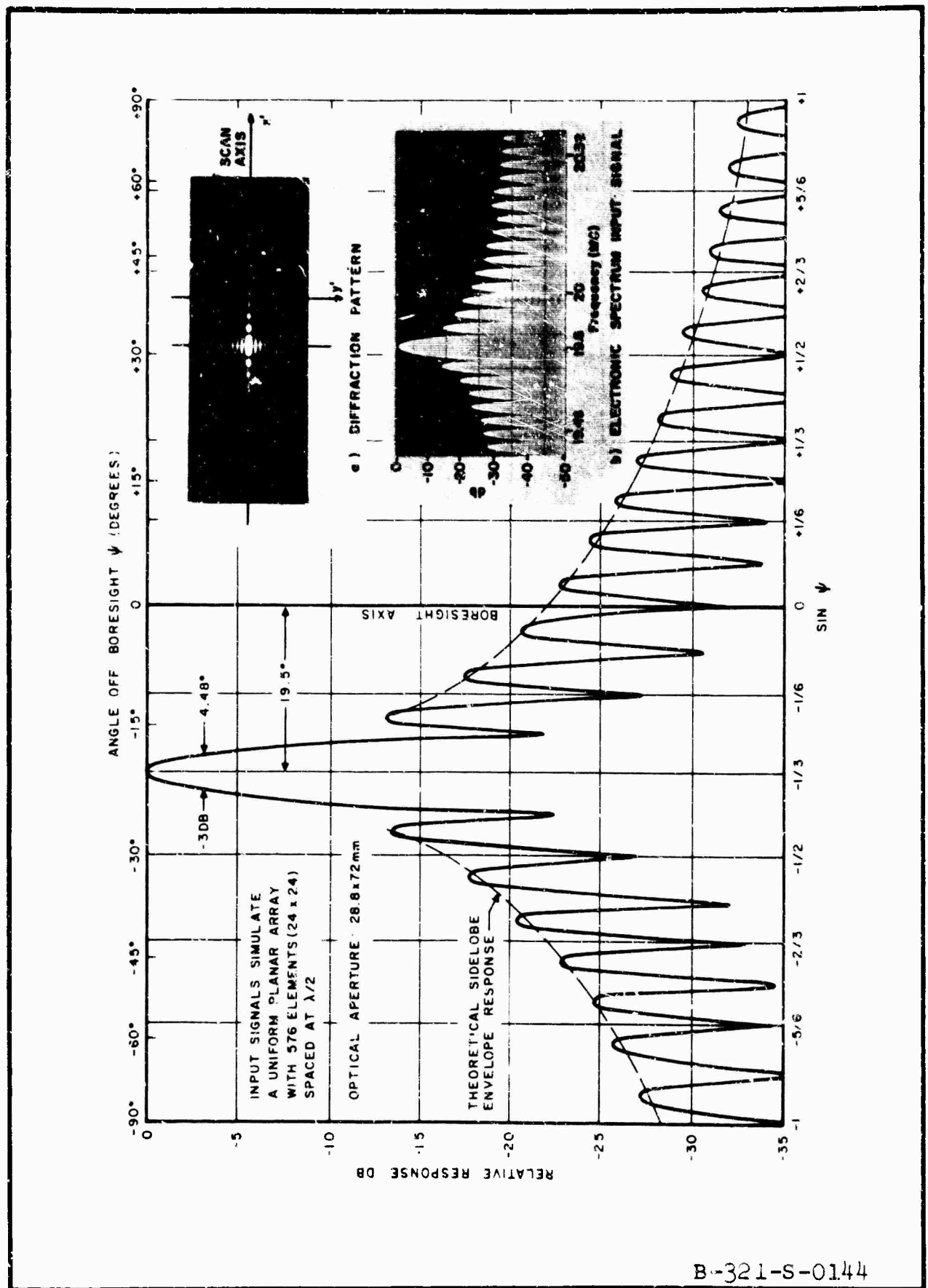


Fig. 10 Planar Array Processor Measured Output Response,  
 $\psi$ -Axis for Simulated Signal at  $(\theta_0 = 0, \psi_0 = -19.5^\circ)$   
 Off Boresight

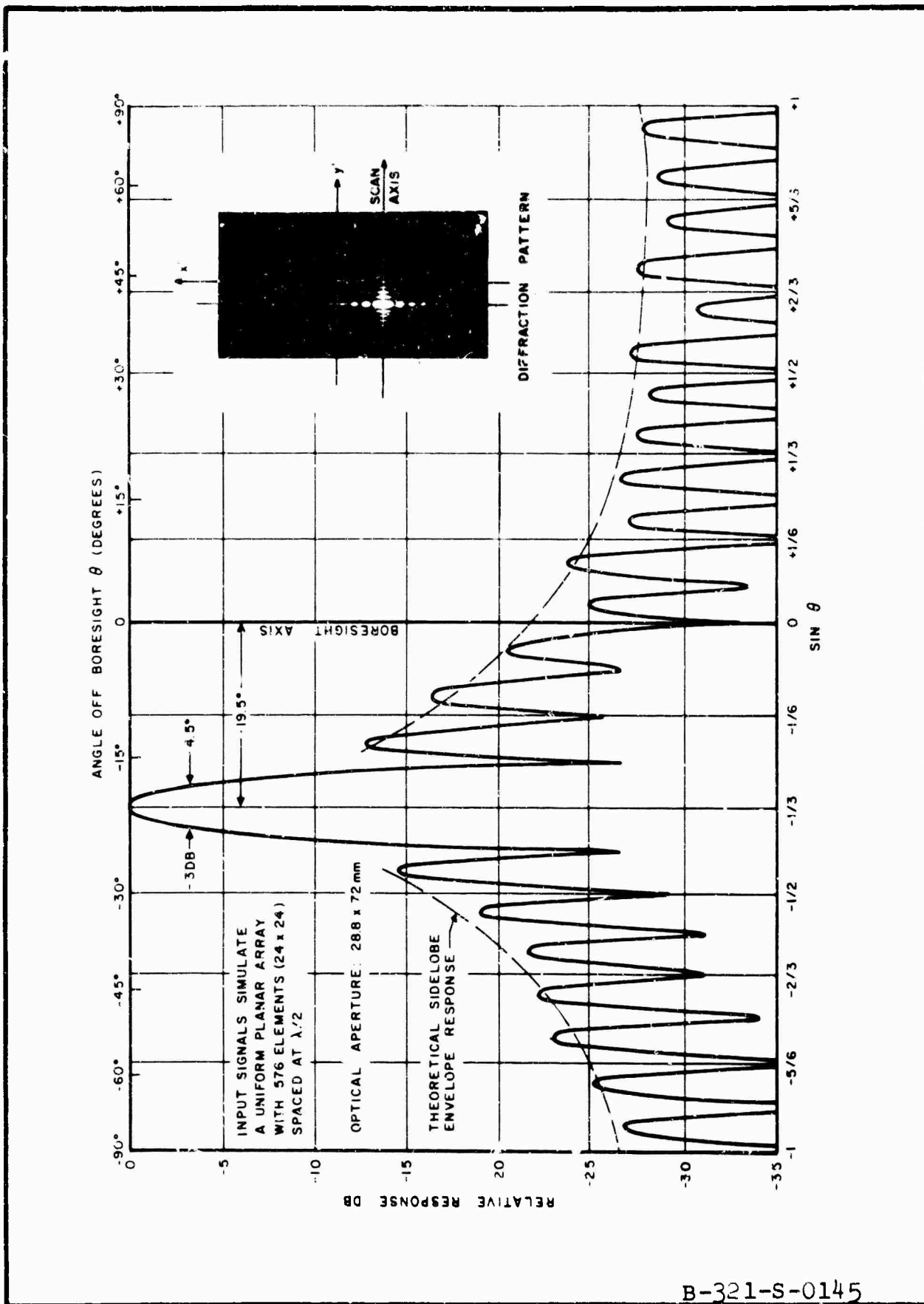


Fig. 11 Planar Array Processor Measured Output Response,  $\theta$ -Axis for Simulated Signal at  $(\theta_0 = -19.5^\circ, \psi_0 = -19.5^\circ)$  Off Boresight

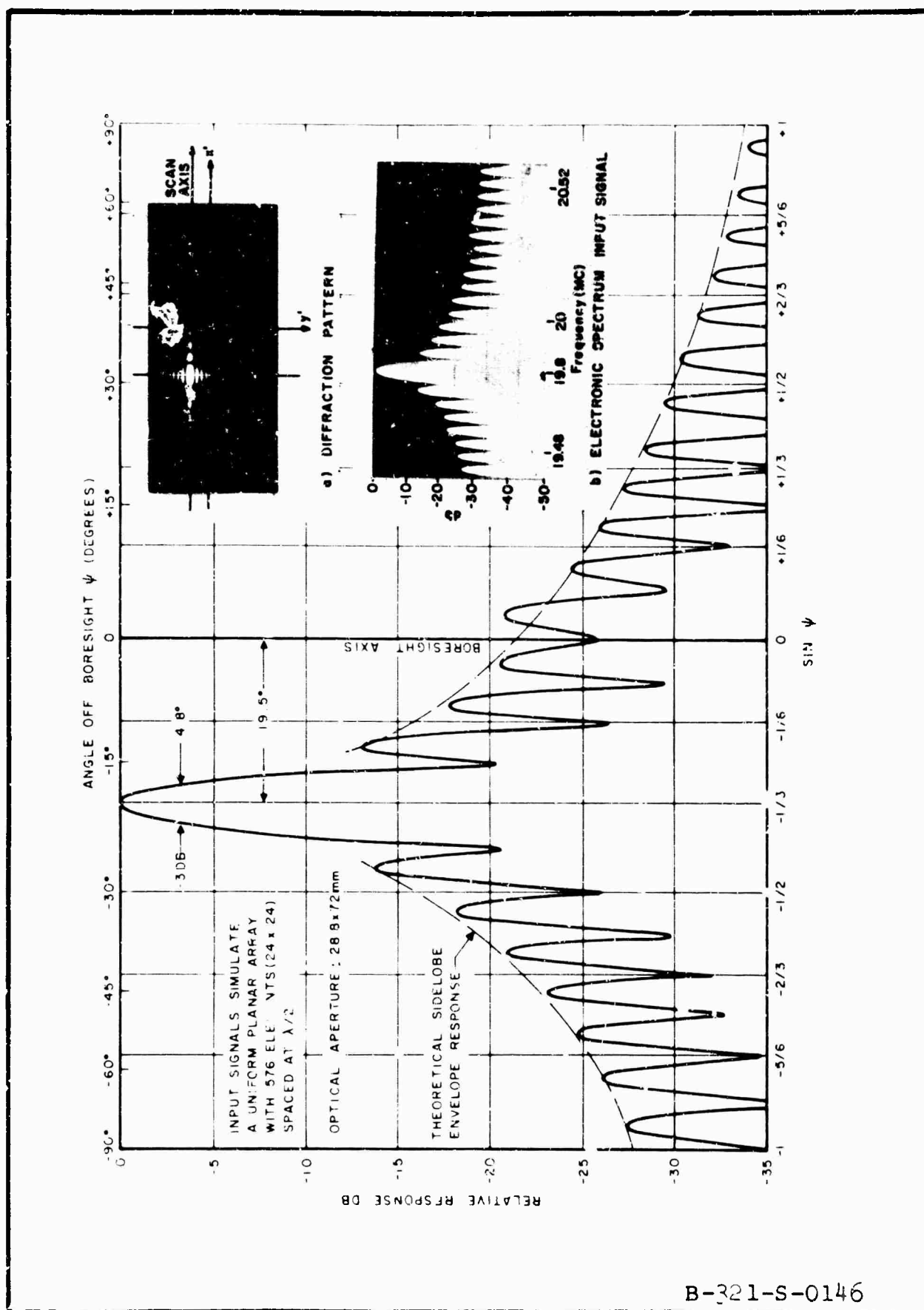
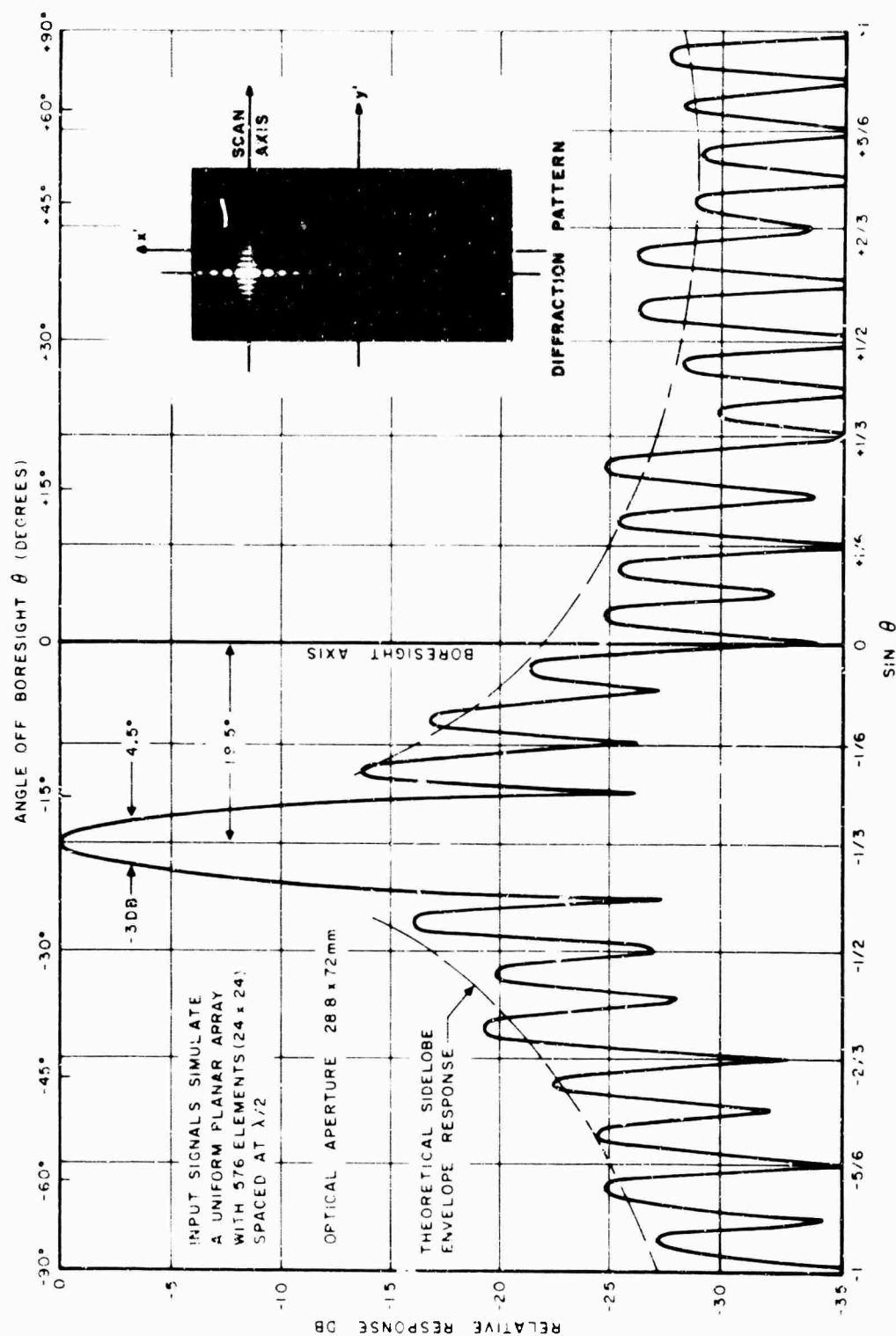


Fig. 12 Planar Array Processor Measured Output Response,  $\psi$ -Axis for Simulated Signal at  $(\theta_0 = -10.5^\circ, \psi_0 = -19.5^\circ)$  Off Boresight



B-321-S-0147

Fig. 13 Planar Array Processor Measured Output Response,  $\theta$ -Axis for Simulated Signal at ( $\theta_0 = -19.5^\circ$ ,  $\psi_0 = +41.6^\circ$ ) Off Boresight

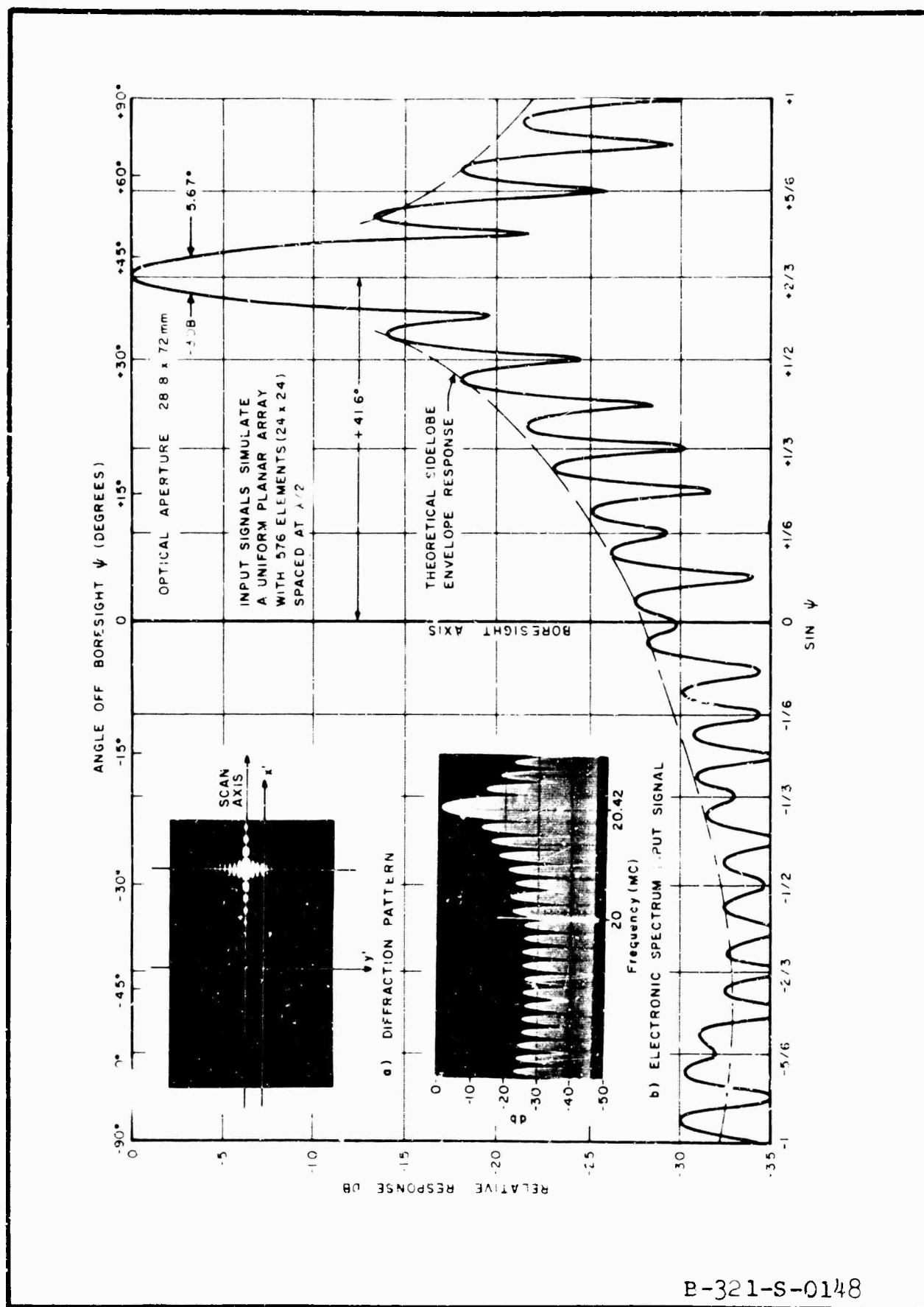


Fig. 14 Planar Array Processor Measured Output Response,  $\psi$ -Axis for Simulated Signal at  $(\theta_0 = -19.5^\circ, \psi_0 = +41.6^\circ)$  Off Boresight

frequency response. The distribution for an off-boresight signal is approximated by the sum of three major light peaks located at 20 mc and  $20 \pm 1.25$  mc in the frequency domain. The experimental frequency response for the multiple transducer is shown in Fig. 15. The curve shows the normalized light peak intensity variation as a function of the input frequency while the voltage input to the transducer is maintained constant. The factors  $A_{\pm 1}$  are evaluated for each value of  $\alpha_1$  and utilized in Eq. 10 to compute the envelope response shown on the experimental results (Figs. 9 - 14).

#### 4. The Spatial Filtering Experimental Results

Figure 16 shows the measured light intensity distribution in the collimated region of the optical system. Since the output focal plane light intensity distribution can be shown to be proportional to the Fourier transform of this aperture distribution, the variations along the aperture appear as sidelobes in the far-field pattern. Figure 17 shows the light intensity distribution along the corresponding output focal plane coordinate for the input given in Fig. 16.

To eliminate these variations a 10-mm focal length microscope objective (Bauch & Lomb) was used to diverge the 5-mm output beam from the laser. Since the light intensity at the focal plane of the objective is the spatial spectrum of the light input, the modulation components of the light were "filtered" with a 20-micron pin hole placed in the focal plane. The measured light distribution in the aperture and in the output focal plane for the spatially filtered light are shown in Figs. 18 and 19, respectively.

Comparing Figs. 16 and 18, and Figs. 17 and 19 shows that the intensity variations were effectively eliminated.

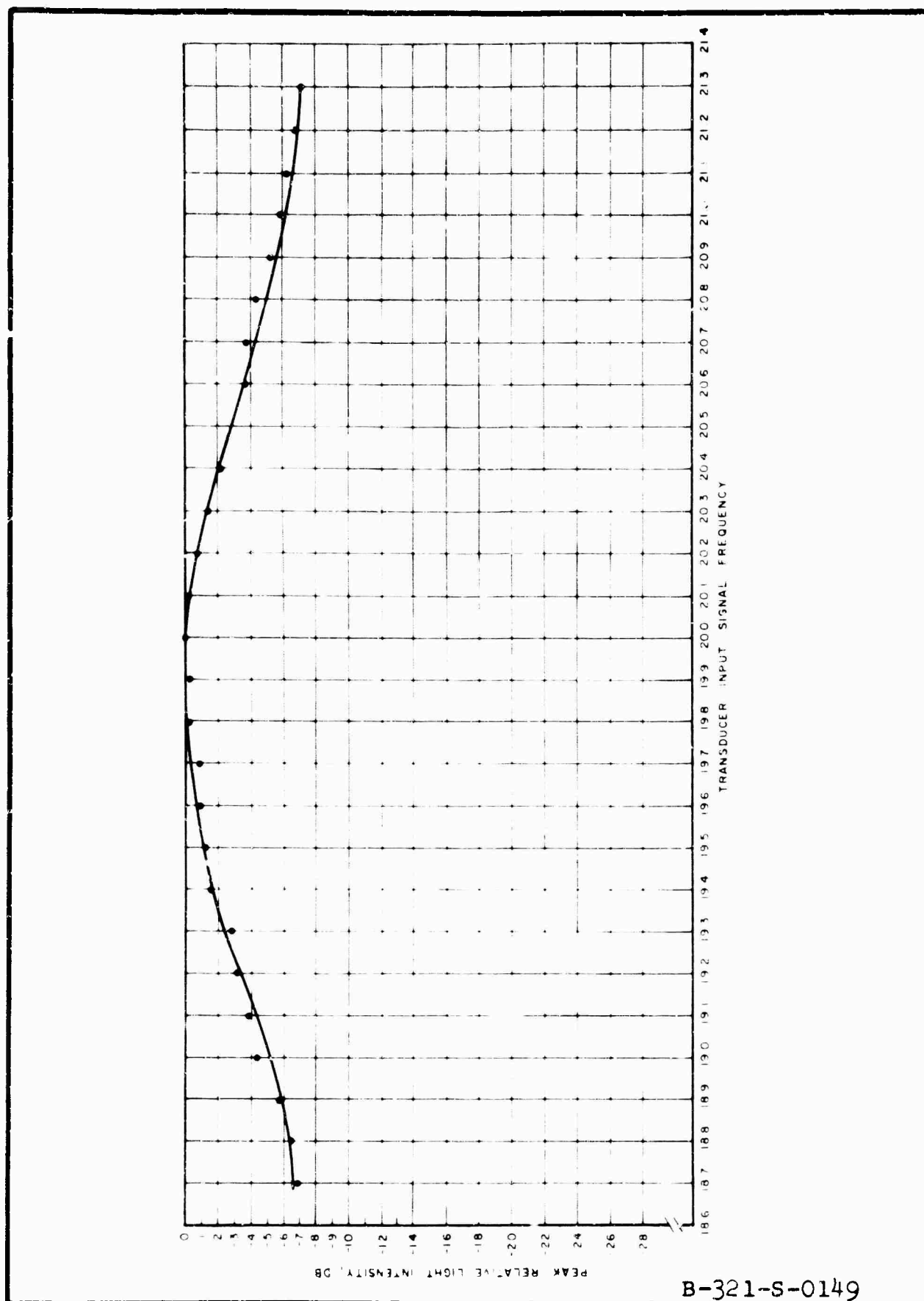


Fig. 15 Experimental Frequency Response of Multiple Channel Transducers



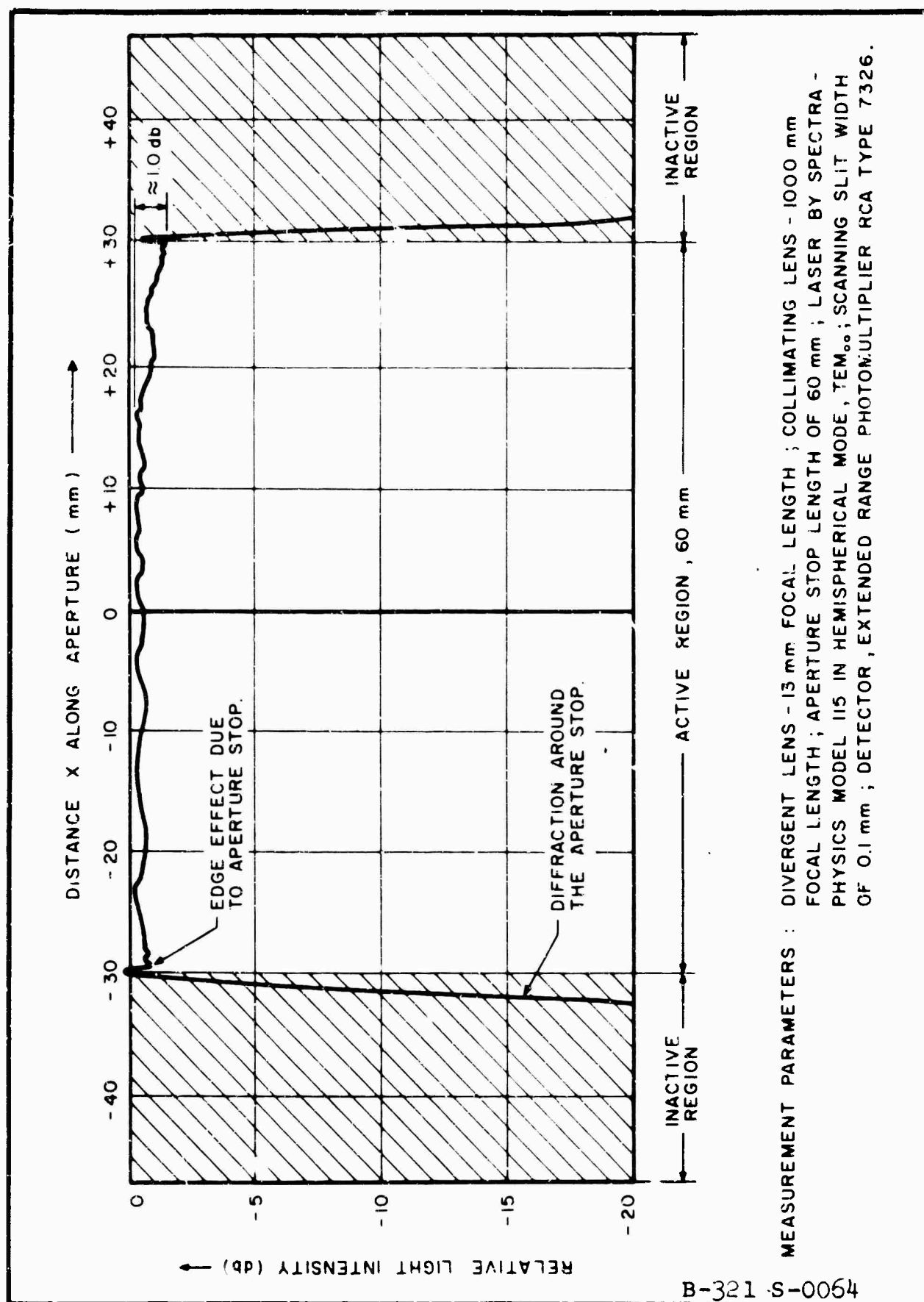


Fig. 16 The Measured Light Intensity Distribution in the Collimated Region of the Optical System

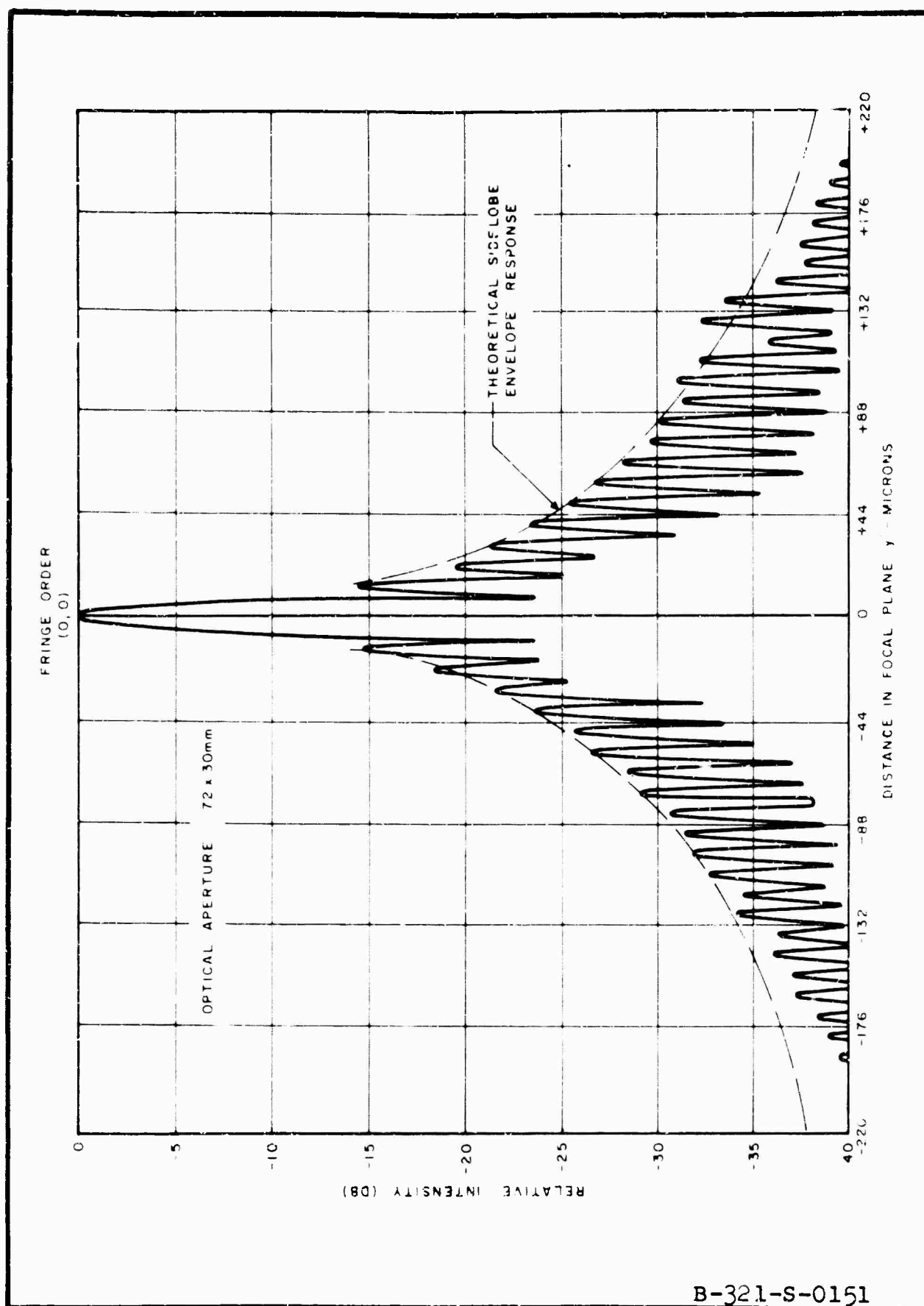


Fig. 17 Zero Order Light Intensity Distribution in Output Focal Plane (Without Spatial Filter)

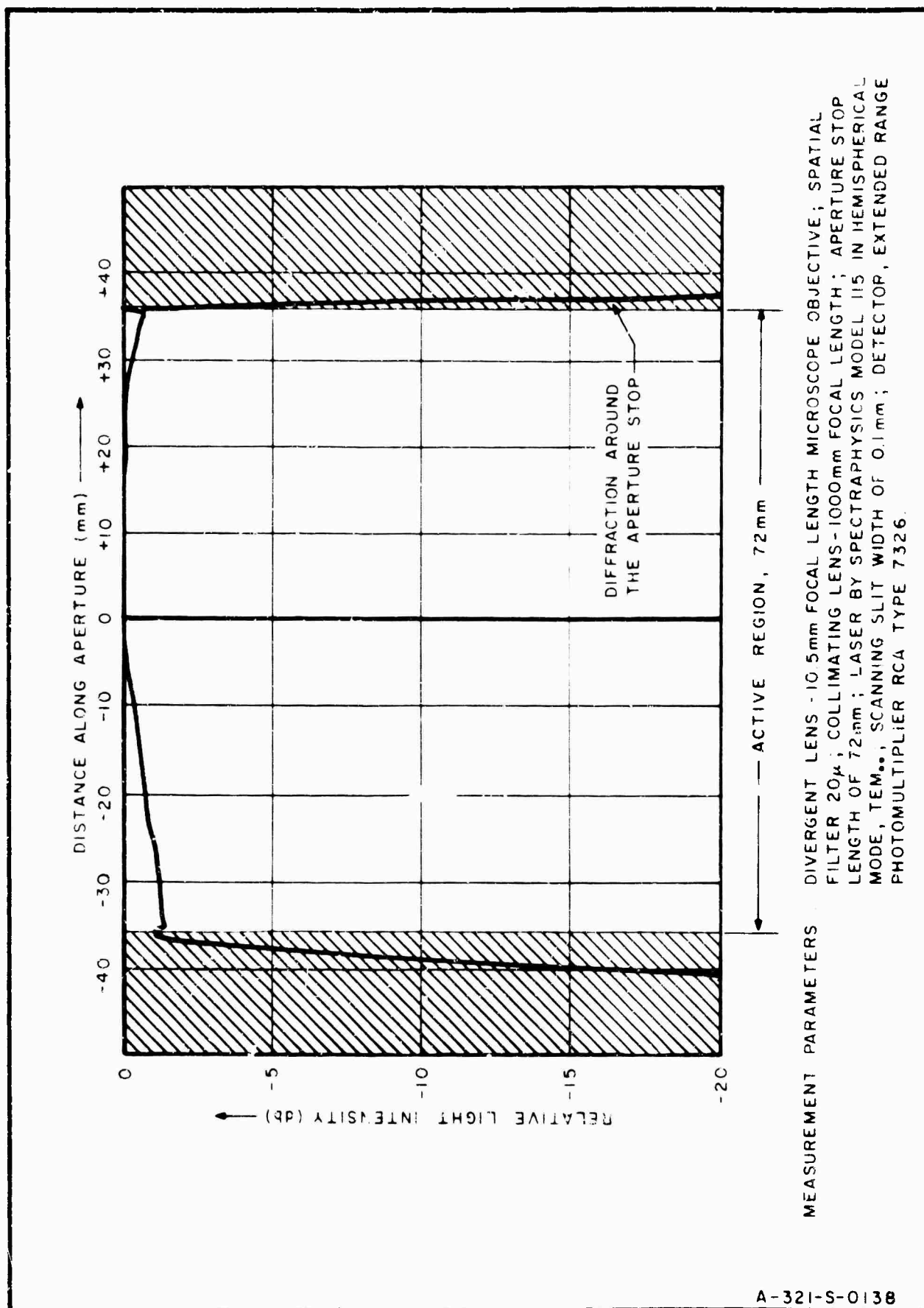


Fig. 18 The Measured Light Intensity Distribution in the Collimated Region of the Optical System (with Spatial Filtering)

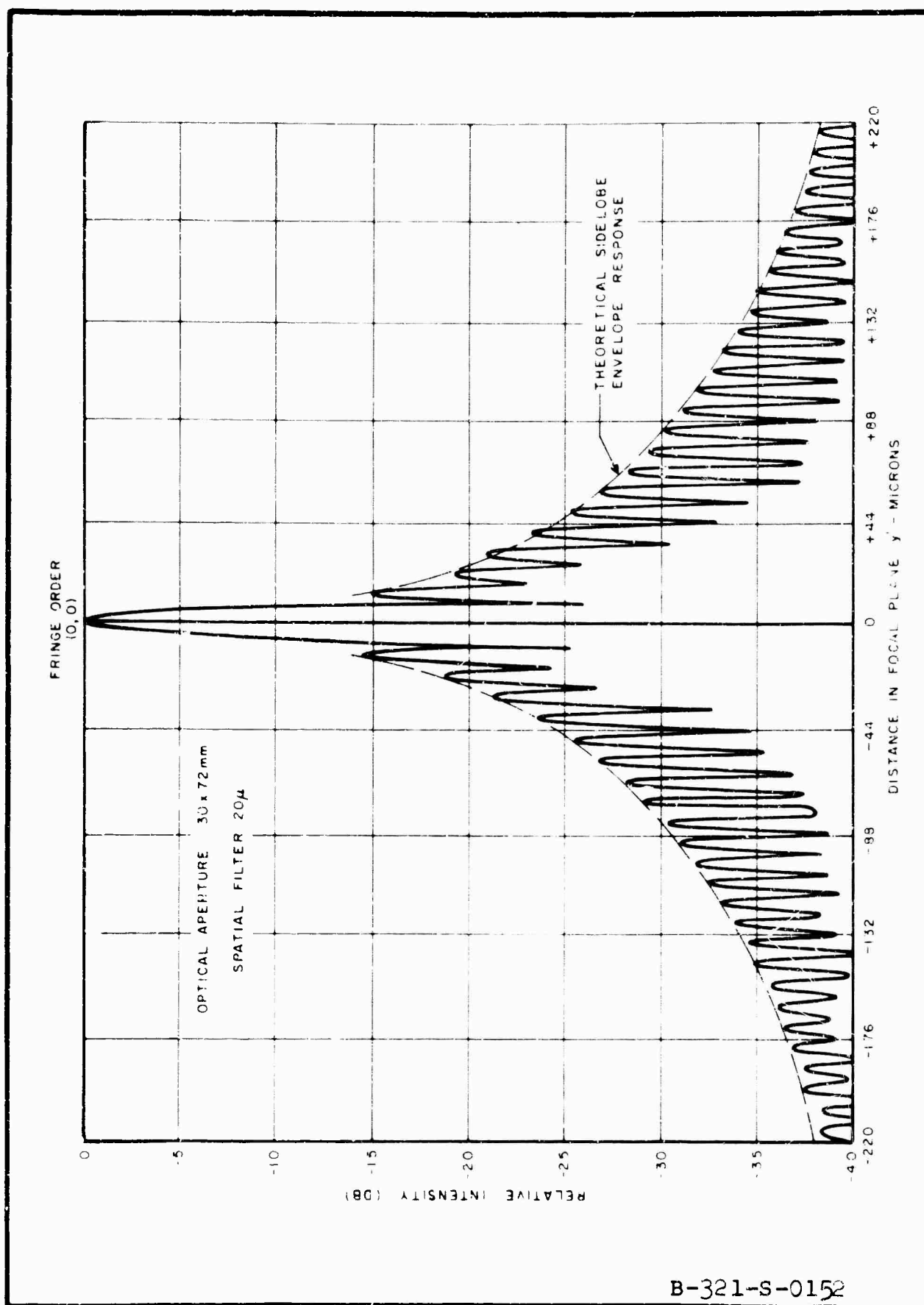


Fig. 19 Zero Order Light Intensity in Output Focal Plane with Spatial Filter

### III. TIME MULTIPLEX SIMULATOR WITH APERTURE WEIGHTING

#### A. AMPLITUDE WEIGHTING - TIME-DELAY MULTIPLEX SIGNAL SIMULATOR

In the time-delay multiplex system, the input to one of the  $N$  ultrasonic light-modulator channels is a pulse train which simulates the time multiplexed output of a linear antenna array, and is given approximately by

$$v_s(t) = \text{rep}_{MT} u(t) = \text{rep}_{MT} \left\{ \sum_{m=-\frac{M-1}{2}}^{+\frac{M-1}{2}} P_T(t-mT) \cdot \cos[2\pi f_o(t-mT) - n\pi \sin \psi_o] \right\} \quad (13)$$

where

$M$  = number of elements in linear antenna array

$m$  = array element index

$$\equiv \begin{cases} 0, \pm 1, \pm 2, \dots, \pm \frac{M-1}{2} & \text{for } M \text{ even} \\ \pm \frac{1}{2}, \pm \frac{3}{2}, \dots, \pm \frac{M-1}{2} & \text{for } M \text{ odd} \end{cases}$$

$T$  = receiver pulse width = multiplexing delay  
between adjacent receiver channels

$$P_T(t-mT) = \begin{cases} 1 & \text{for } |t-mT| < T/2 \\ 0 & \text{for } |t-mT| > T/2 \end{cases} \quad (14)$$

$f_o$  = intermediate frequency of receiver

$\psi_o$  = angle between target and boresight axis of  
linear antenna array

and

$$\text{rep}_{MT} u(t) \equiv \sum_{k=-\infty}^{+\infty} u(t-kMT) \quad (k = 0, \pm 1, \pm 2, \dots)$$

In terms of this signal, the ultrasonic cell acts as a time "window" of width  $MT$  seconds which scans  $v_s(t)$  in the direction of increasing time. In sliding from  $u(t-kMT)$  to  $u[t-(k+1)MT]$ , the signal in the cell corresponds to the input:

$$P_{MT}(t-\gamma) v_s(t)$$

where

$$kMT \leq \gamma \leq (k+1) MT$$

the angle  $\psi_0$  is limited to discrete values such that the phase information  $n\pi \sin \psi_0$  in  $v_s(t)$  repeats every interval  $MT$ . In this case, the light intensity distribution in the output focal plane (magnitude squared of the Fourier transform of Eq. (14)) is independent of  $\gamma$ . Only a phase shift is involved.

The focal plane spectrum for the object plane distribution, Eq. (14), has a peak side-lobe level only 13.2 db below the central lobe peak. To decrease the sidelobe level it is desirable to amplitude weight this aperture distribution.<sup>5</sup> In order to weight the aperture distribution of each light modulator channel with a Hamming-type function, the time-multiplexed signal input to this channel must be sinusoidally amplitude modulated with period equal to the channel delay  $MT$ , in synchronism with the multiplexing. The modulation (normalized) is of the form:

$$T_a(t) = \text{rep}_{MT} m(t) = \text{rep}_{MT} \left\{ [a + (1-a) \cos \frac{2\pi}{MT} t] P_{MT}(t) \right\} \\ = [a + (1-a) \cos \frac{2\pi}{MT} t] (\text{continuous}) . \quad (15)$$

The pedestal height  $h$  of the modulation is the minimum normalized amplitude at  $t = \pm(2k+1) \frac{MT}{2}$ , and is related to  $a$  by:

$$h = 2a - 1 . \quad (16)$$

In the case of aperture weighting, the light intensity distribution in the output focal plane is no longer independent of  $\gamma$ . To show this, it suffices to consider the simple case of  $\theta = 0$  and  $T = \frac{1}{f_0}$  in Eq. (13), which then reduces to a pure carrier:

$$v_s(t) = \text{rep}_{MT} [P_{MT}(t) \cos 2\pi f_0 t] = \cos 2\pi f_0 t \quad (17)$$

weighting this signal according to Eq. (15), we have:

$$v_{SM}(t) = v_s(t) T_a(t) = [a + (1-a) \cos \frac{2\pi}{MT} t] \cos 2\pi f_0 t \quad (18)$$

the aperture signal is now:

$$P_{MT}(t-\gamma) v_{SM}(t) \quad (19)$$

$$\text{or} \quad P_{MT}(t) v_{SM}(t-\gamma) \quad (20)$$

Equation (20) considers the signal as sliding with respect to a fixed "window." Using (20), the complex transmission function

for the delay line light modulator may be approximated, for small phase modulation index  $\psi_m$ , by:

$$T(\tau) = P_{MT}(\tau)[1 + j\psi_m \cos 2\pi f_o(\tau - \gamma)] \quad (21)$$

where:

$\tau \equiv$  normalized input space variable<sup>2</sup>

$$\psi_m \equiv k_s[a + (1-a) \cos \frac{2\pi}{MT}(\tau - \gamma)] \quad (22)$$

$k_s \equiv$  constant .

The resulting light intensity distribution at the output focal plane is:

$$I(r, m, \gamma) = \left\{ \text{sinc}^2 r \right\} \left\{ 1 + \frac{m^2 r^2}{2} \left[ \frac{r^2 + 1}{(r^2 - 1)^2} \right] - \frac{2mr^2}{r^2 - 1} \cos w_1 \gamma + \frac{m^2 r^2}{2(r^2 - 1)} \cos 2w_1 \gamma \right\} \quad (23)$$

where

$$r = uMT$$

$u \equiv$  normalized output focal plane variable<sup>2</sup>

$$m = \frac{1 - a}{a}$$

$$w_1 = \frac{2\pi}{MT} \quad .$$

Equation (23) verifies that the output light intensity distribution is a function of  $\gamma$ , except at the central peak ( $r = 0$ ) and at the side lobe nulls. Note the presence, in addition to the fundamental frequency  $w_1$ , of a second harmonic  $2w_1$ . The order of magnitude of these AC components is shown by the solution of (23) for the second side-lobe peak ( $r = 2.5$ ) with pedestal height  $h = 0.2$  ( $a = 2/3$ ):



$$I(2.5, 0.67, \gamma) = \frac{1}{233} [5.16 - 6 \cos w_1 \gamma + \cos 2w_1 \gamma] . \quad (24)$$

Note first that the second harmonic is one-sixth of the fundamental. Plotting this equation (Fig. 20) on a log scale, we note that the variation is approximately 20 db. The minima occurs at  $\gamma = 0$ . It is these minima we must record. To do so, it is necessary to sample the output at  $\gamma = 0$  with periodicity  $T_1 = 19.2 \mu\text{sec}$ .

Since we cannot sample in zero time, it is necessary to know the error incurred by a sample of duration  $T_2$ . To find this error, we define

$$R(T_2) = \frac{I_{\text{avg}}(\gamma, T_2)}{I_0} \quad (25)$$

$$I_{\text{avg}}(\gamma, T_2) = \frac{1}{T_2} \int_{-\frac{T_2}{2}}^{+\frac{T_2}{2}} I \, d\gamma$$

$I_0$  = desired value of  $I$  at  $\gamma = 0$ .

The solution of (25) is:

$$R\left(\frac{T_2}{T_1}\right) = \frac{\left(\frac{A_3(r, m) T_2}{\pi T_1}\right) \left(\sin \pi \frac{T_2}{T_1}\right)}{A_1(r, m) + A_2(r, m) - A_3(r, m)} \quad (26)$$

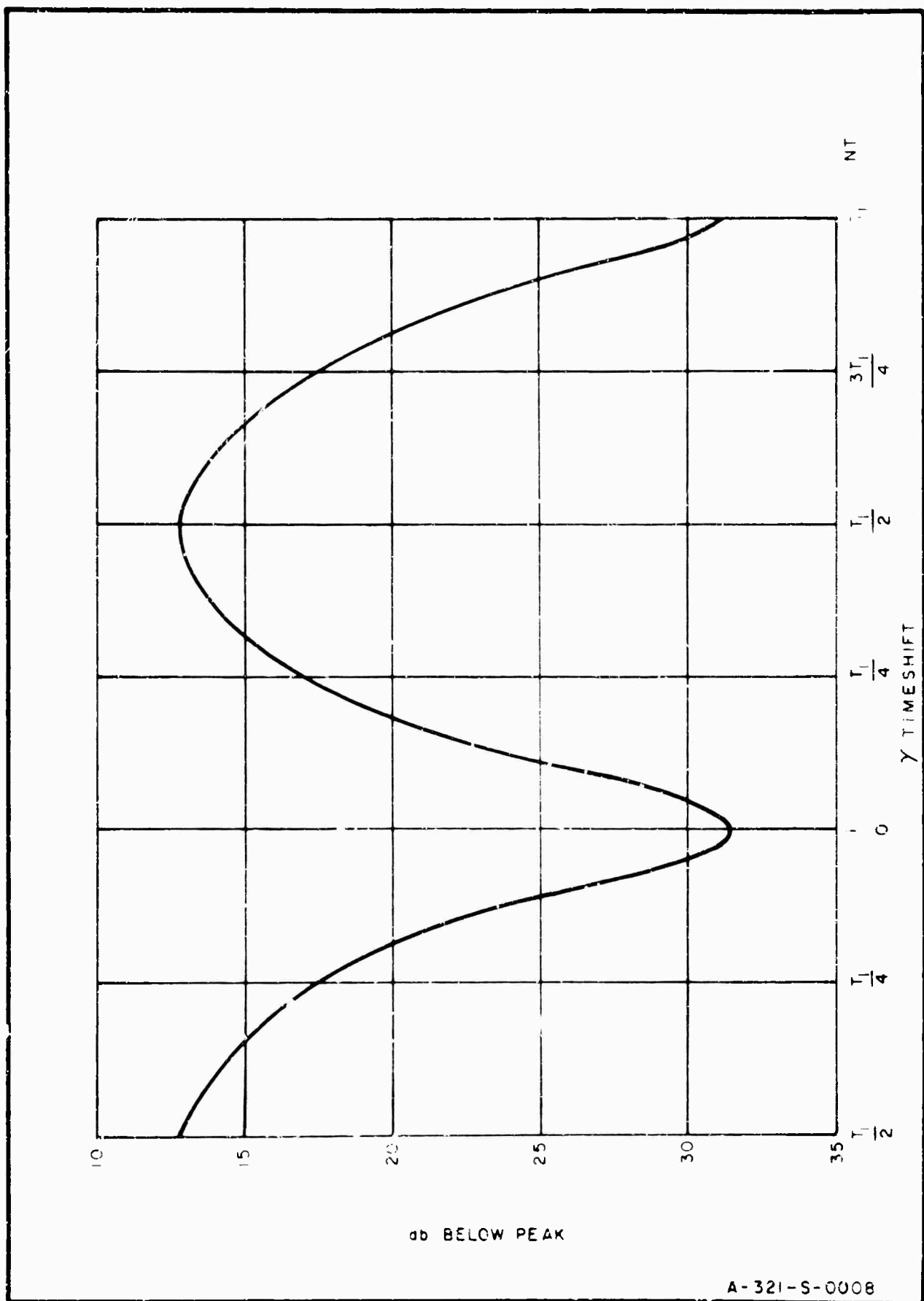


Fig. 20 Variation of 2nd Sidelobe of Output Focal Plane Light Distribution as a Function of Aperture Shift

where:

$$A_1(r, m) \equiv [r^2 - 1 + \frac{m^2 v^2}{2} (\frac{r^2 + 1}{r^2 - 1})]$$

$$A_2(r, m) \equiv \frac{m^2 r^2}{2}$$

$$A_3(r, m) \equiv 2mr^2 .$$

Figure 21 is a plot of this result for the second side lobe. From the figure, we deduce that for a sample time of one-tenth the sample interval  $T_1$ , we incur a 0.8 db error.

In summary, to simulate a weighted time-multiplexed system, additional circuitry must be provided which:

- (1) Synchronously amplitude-modulates the time-multiplexed signal.
- (2) Samples the time-varying output when the aperture distribution is appropriate.

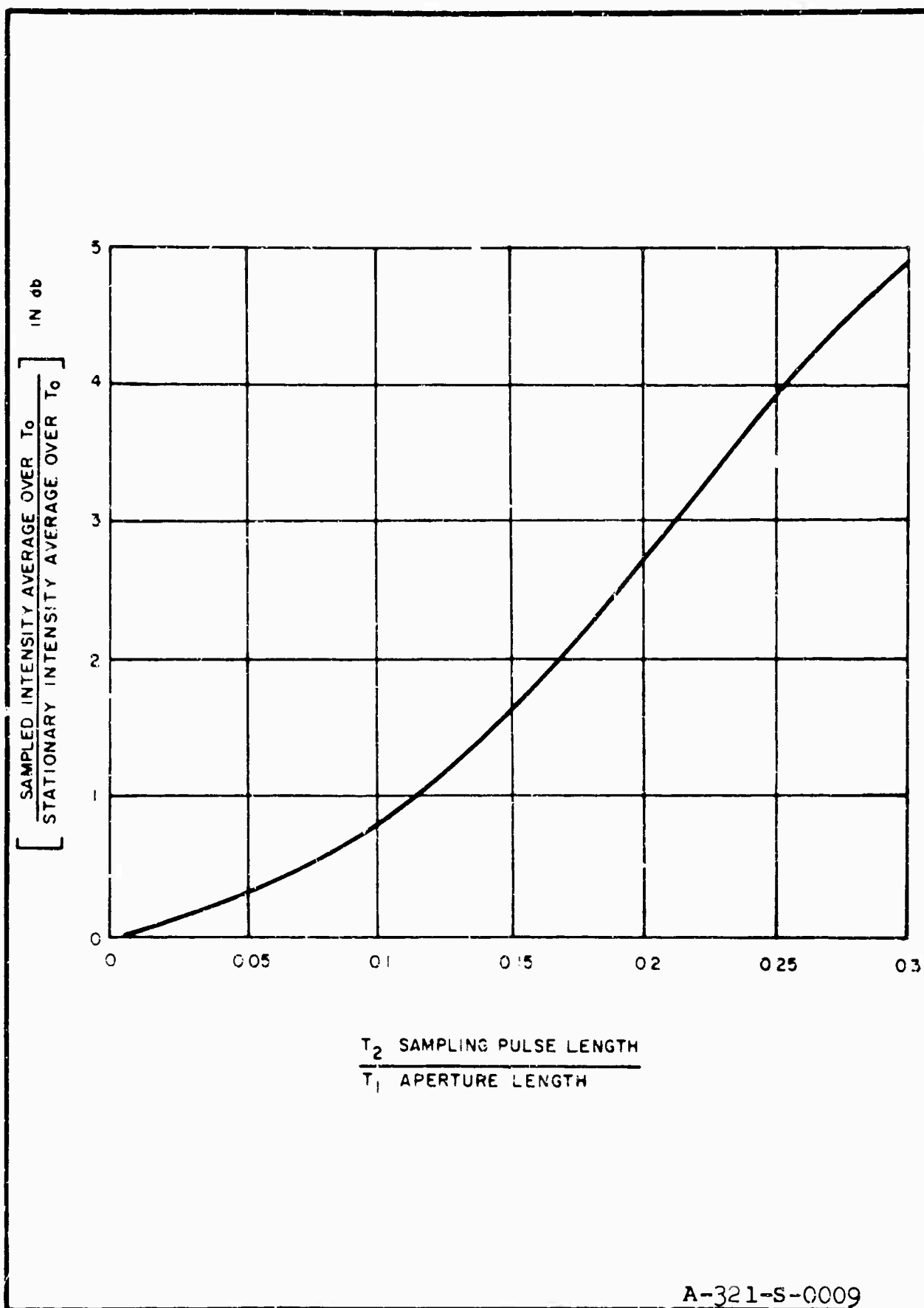
#### B. THE IMPLEMENTATION OF AMPLITUDE WEIGHTING FOR THE TIME DELAY MULTIPLEX SIGNAL SIMULATOR

For ease of reference, the block diagram of the time-multiplexed signal simulator is recreated in Fig. 22. For this discussion, note that 12 channels simulate 24 signals, 2 cycles of the ring counter constituting one interrogation of  $M = 24$  antenna array elements. This is possible if the antenna phase pattern repeats every 12 elements.

Note also that the sampling time  $\gamma = 0$  occurs when Gate 1 goes ON (Gate 12 goes OFF).

##### 1. Weighting of the Time Multiplexed Signal (Fig. 23)

The modulation is derived from the leading edge of the gate pulse to channel  $n$ . The reason for this choice will

Fig. 21 First Sidelobe Level Increase as Function of  $T_2/T_1$

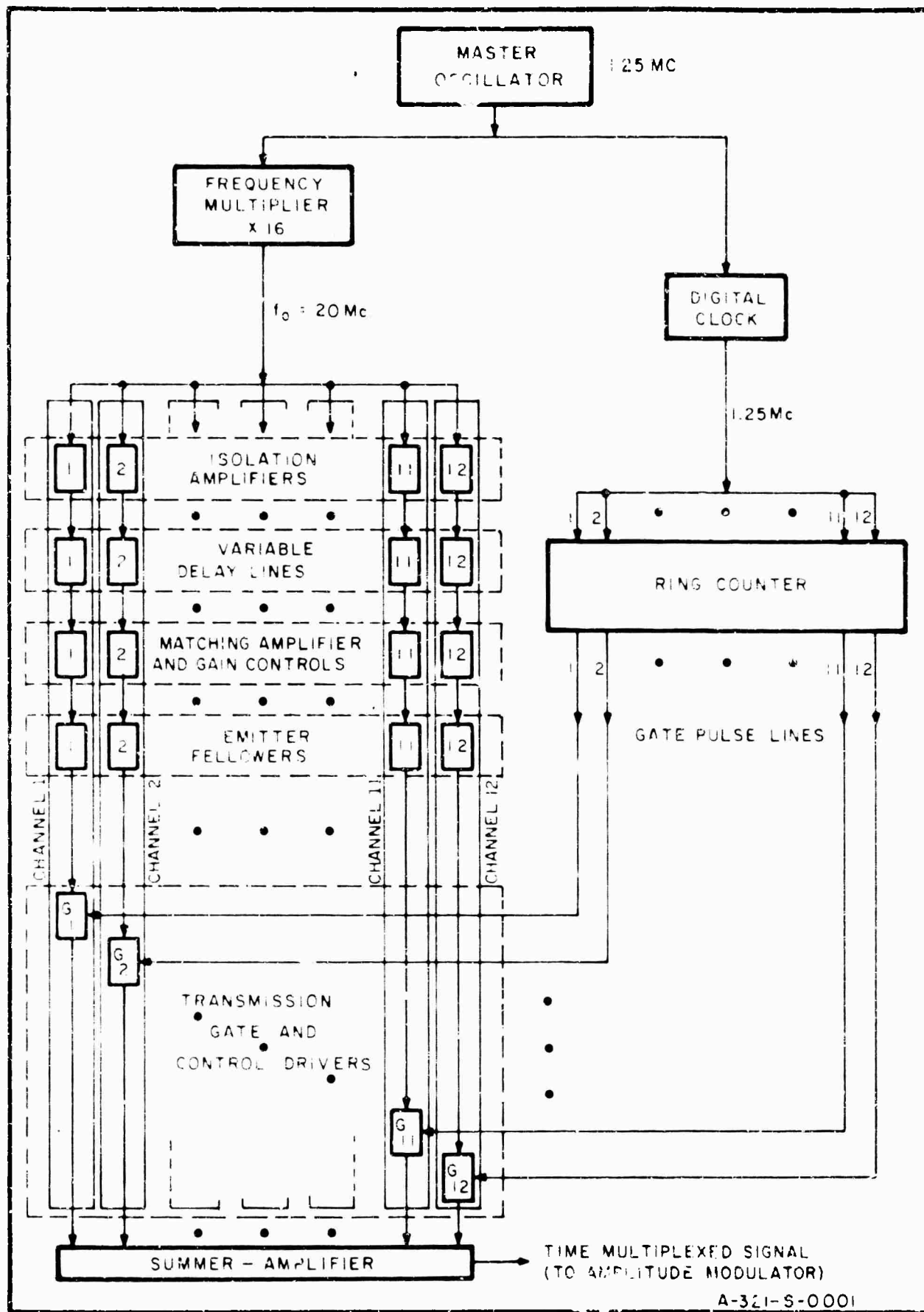


Fig. 22 Block Diagram of Signal Simulator to Generate a Time-Multiplexed Waveform

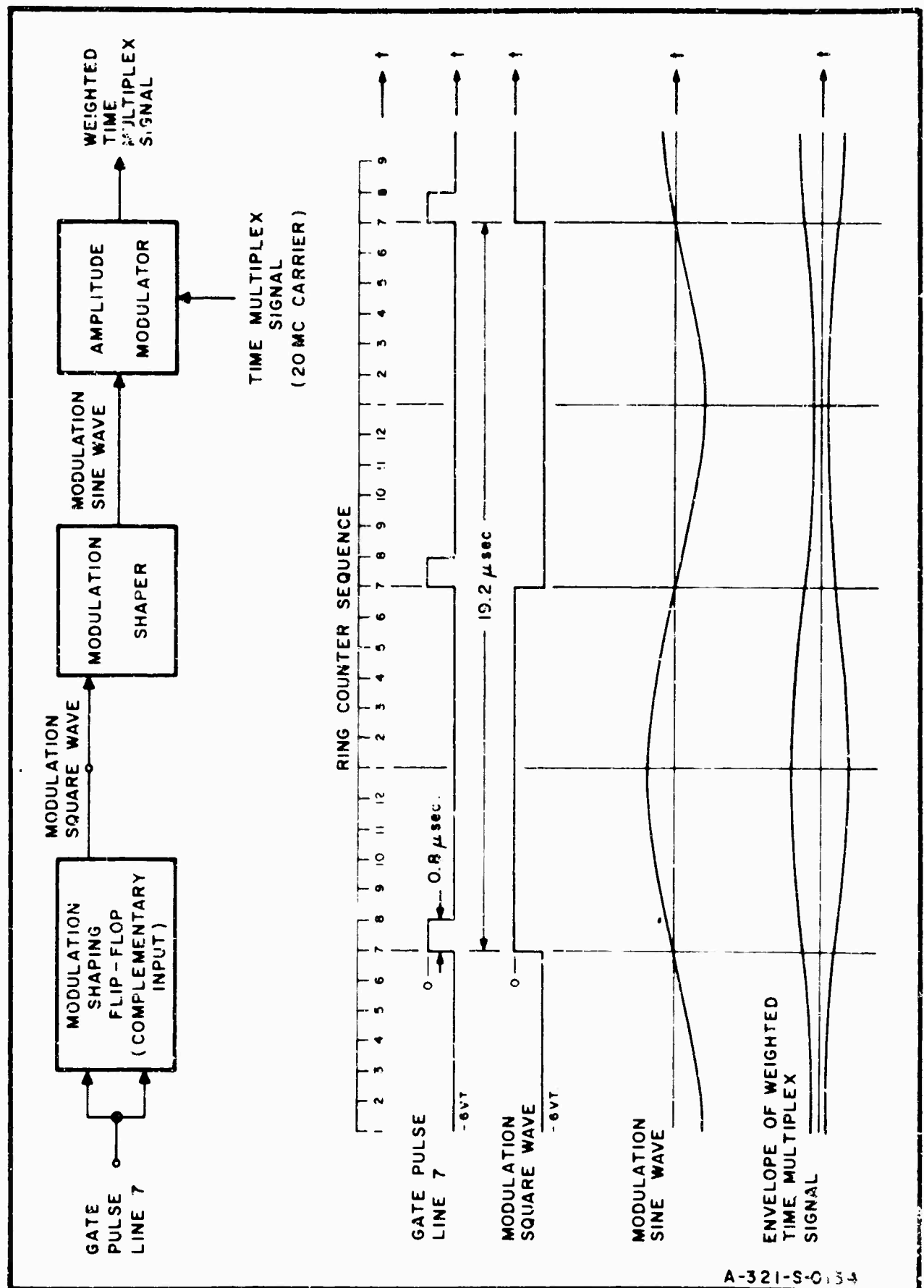


Fig. 23 Time-Multiplex Signal Weighting Block Diagram and Waveforms

appear shortly. The pulse train on Gate Pulse Line 7 has a pulse width of  $0.8 \mu\text{sec}$  and a period of  $12 \times 0.8 \mu\text{sec} = 9.6 \mu\text{sec}$ , since the time-multiplexed system has 12 gates. This signal triggers a complementary flip-flop. The output of the flip-flop is a square wave of period  $19.2 \mu\text{sec}$ . In the Modulation Shaper (Fig. 24), the square wave is passed through a high-Q tank circuit tuned to 52 kc. Hence all the harmonics of the square wave are filtered out, and the 52 kc fundamental suffers negligible phase shift. The maxima and minima of the output are synchronous with the start of Gate pulse 1, as required. High-Q is obtained by driving the tank with a high-impedance source Q1, and loading it with a high-impedance load, the Darlington Stage Q2 - Q3.

The modulation is applied to the emitter of the common-emitter amplifier in the low-level Amplitude Modulator<sup>9</sup> (Fig. 24) whence the emitter-base potential is varied, thereby modulating the transconductance of the transistor. When the modulation is a positive maximum, the emitter-base potential is a maximum, the transconductance is a maximum, and the output is a maximum. The envelope of the output is hence in phase with the modulation. The modulation is linear only at low levels, hence the carrier input must be attenuated to about 0.14 volts peak, while for 100 per cent modulation the modulation input is about 0.15 volts peak. The average transconductance, determined by the bias point, is varied with the GAIN LEVEL CONTROL.

## 2. Sampling of Spectrum (Fig. 25)

The spectrum signal appears at the output of the photomultiplier, which is essentially a current source. The dynamic range of this current is four (4) decades (from below  $10^{-7}$  amperes). Since the photomultiplier scans a

P-3/321



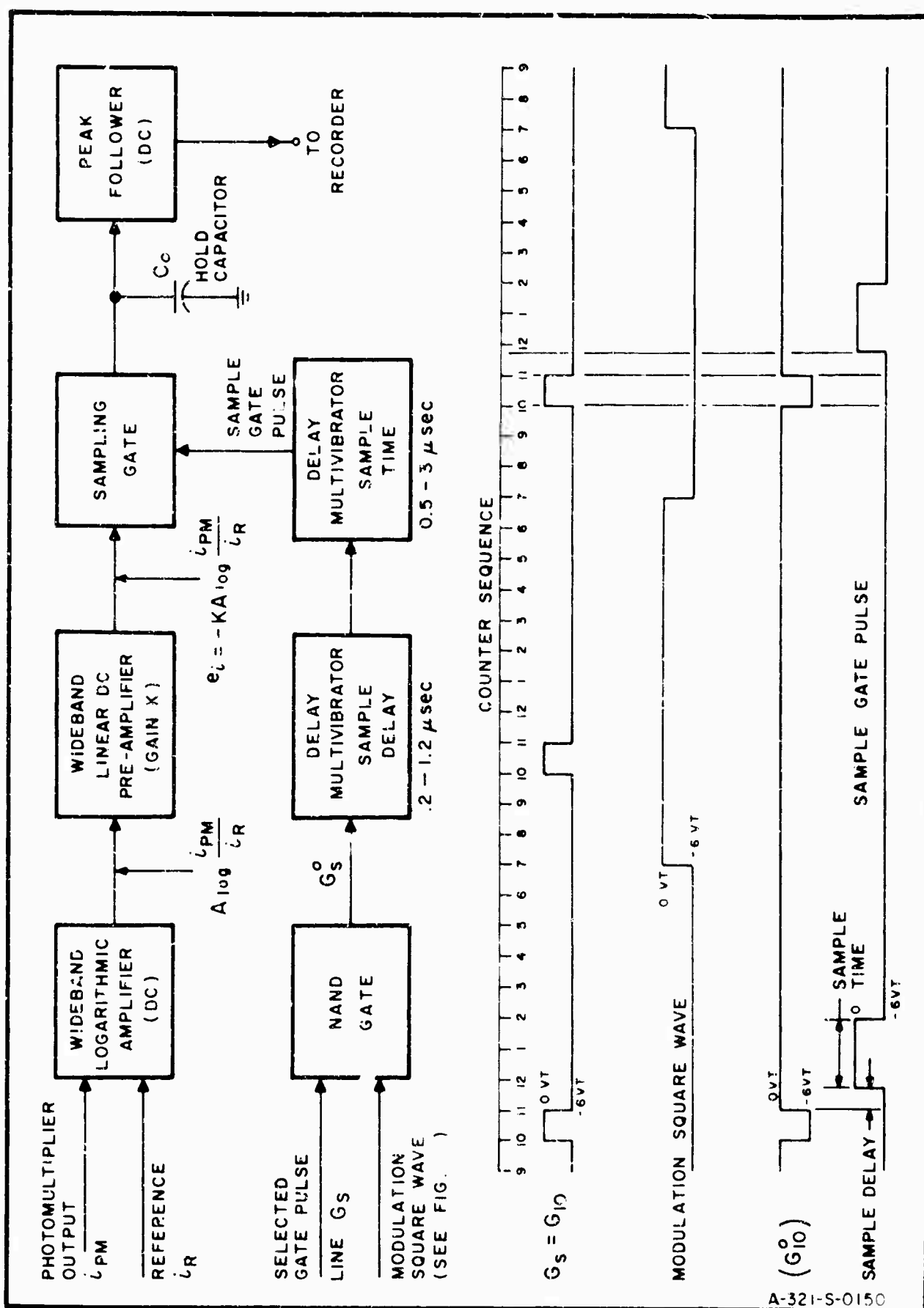


Fig. 25 Spectrum Sampling Block Diagram and Waveforms

1- $\mu$  slit slowly (estimated at 0.4 sec), and since the sampling interval is 19.2  $\mu$ sec the photomultiplier current  $i_{pm}$  will contain a large number of samples (estimated at 20,000) of each "point" on the envelope of the focal plane spectrum. However, at each such "point,"  $i_{pm}$  varies periodically with a 52 kc fundamental and a small second harmonic (Eq. 24).

It was not feasible to gate this signal directly with accuracy. The dynamic range is too great. The range was reduced by taking the logarithm of  $i_{pm}$  (Fig. 26). The photomultiplier dark current  $i_p$  may be compensated for by an adjustable reference current  $i_R$ . Or  $i_R$  may furnish an index level or threshold. The differential operational amplifier is equipped with logarithmic feedback in the form of a transistor (operated as a diode).<sup>10</sup> The amplifier must have input error current much less than the lowest current of interest and gain-bandwidth large enough such that at the highest frequency of interest, the gain is sufficient to keep the differential input error voltage small. If not, the response departs from log-linearity. In addition, the differential input impedance must be high (estimated at 2.5 megs). The Philbrick P-35A Amplifier was selected as best approaching these requirements. In dynamic tests, as recommended by Gibbons and Horn,<sup>10</sup> the amplifier responded at 52 kc with an error of 1 db and at 10<sup>4</sup> kc with an error of 3 db. In DC tests, a plot of output vs  $\log i_{pm}$  was linear over the required 4 decade range with a slope of 60 mv/decade.

The logarithmic unit consisted of two matched transistors in a common heat sink. This is necessary to compensate for the temperature sensitive leakage current of the transistor.

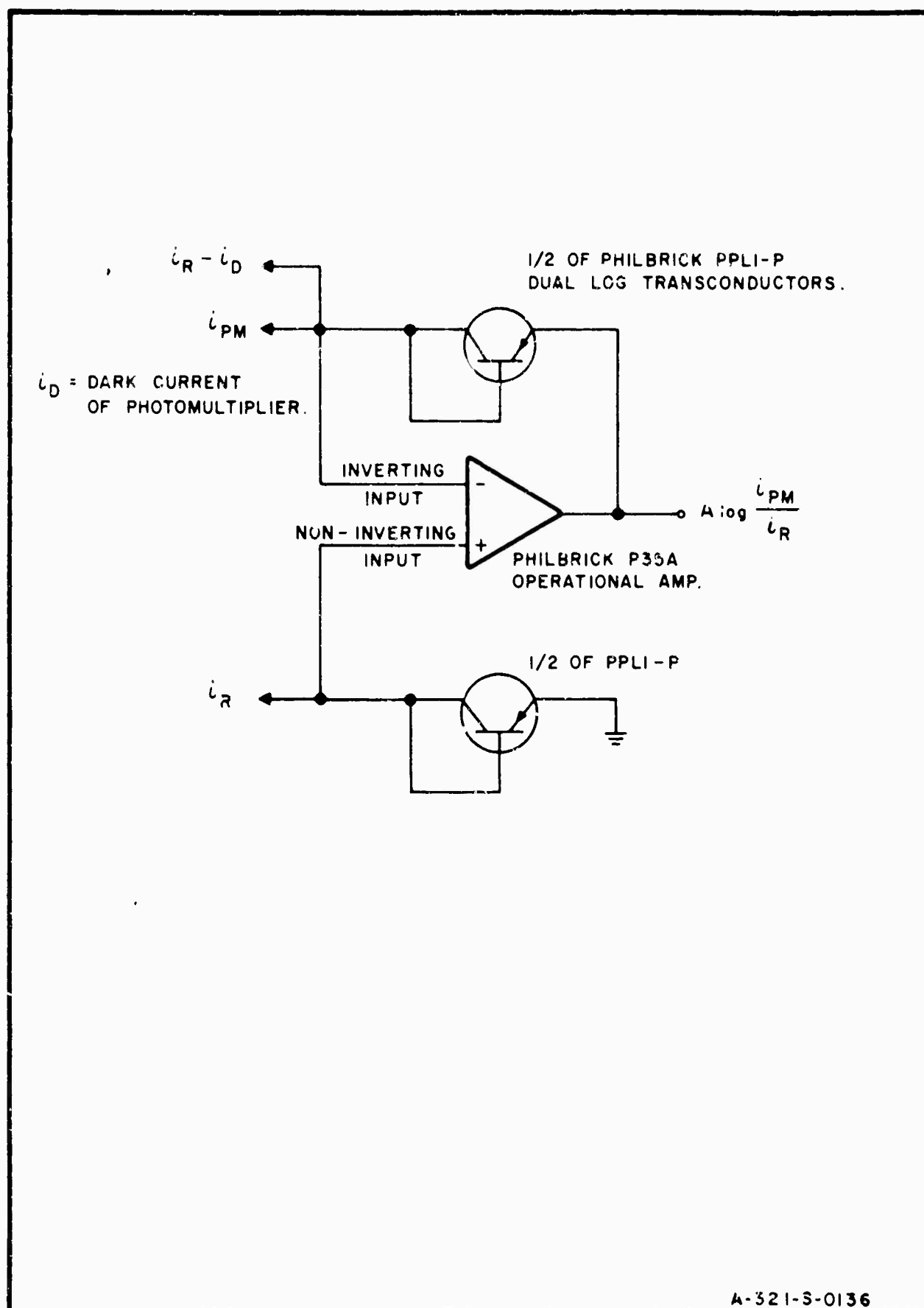


Fig. 26 Logarithmic Amplifier

A DC amplifier is required since the spectrum main peak and nulls are time-invariant.

Sampling is accomplished by a fast sample and hold circuit<sup>11</sup> (Fig. 27). The output of the log amplifier is amplified by a conventional linear DC operational amplifier to a level larger than the subsequent sample gating transients. The low output impedance of the linear pre-amplifier permits fast charging of the holding capacitor when sampling.

The sampling gate is controlled by a signal derived from a selected GATE PULSE LINE. As illustrated in the waveforms, the selection is based on the requirement that, after suitable delay, the center of the sample GATE PULSE falls at the start of channel I gating. Both the SAMPLE DELAY AND SAMPLE GATE PULSE width are continuously variable by means of monostable multivibrators.

The SAMPLING GATE is similar to the GATE CONTROL DRIVER and TRANSMISSION GATE.<sup>6</sup> The only difference is that in the sampling gate the voltage swings seen by the diode gate are reduced to minimize switching transients. Since the  $\delta$ -diode transmission gate is bi-directional, the holding capacitor will charge for  $e_i > e_o$  and discharge (with the same time constant) for  $e_i < e_o$ . The value of  $C_o$  is chosen to permit  $e_o$  to attain the level  $e_i$  during photomultiplier scan of a 1- $\mu$  slit. Between samples,  $C_o$  must see a very high impedance, since (a) this interval is as much as 20 times the sample time and  $C_o$  cannot lose its charge between samples, and (b) such a loss of charge between samples is level dependent, causing a nonlinearity. The high impedance is provided by a differential amplifier wired as a follower.

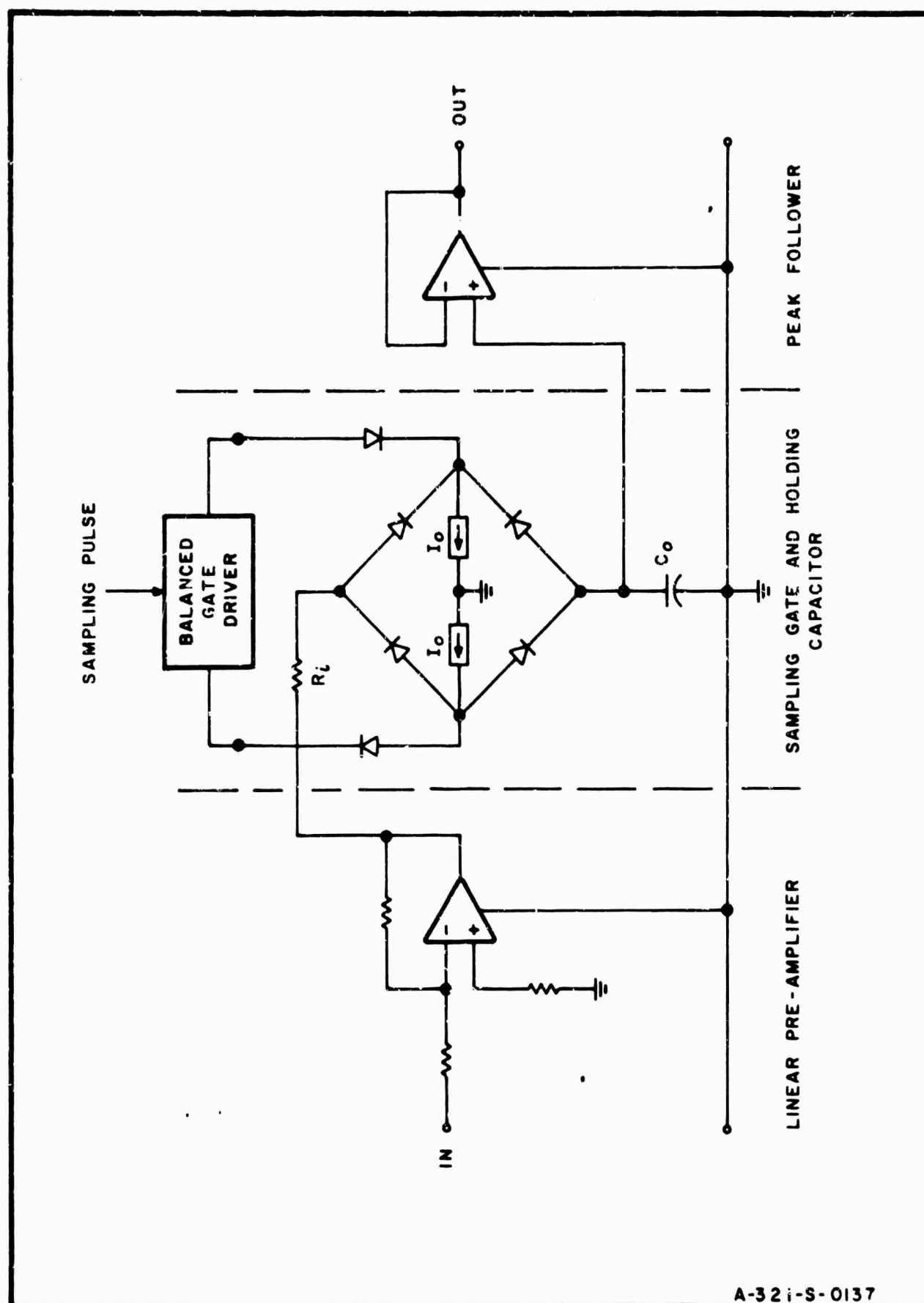


Fig. 27 Sampling System

COLUMBIA UNIVERSITY—ELECTRONICS RESEARCH LABORATORIES

The small resistor  $R_1$  improves preamplifier stability under switched load conditions. Using constant current generators  $I_0$  to supply the gate current insures that the gate presents a high impedance to the driver at all times.

IV. REFERENCES

References 1 through 8 were prepared at the Electronics Research Laboratories, School of Engineering and Applied Science, Columbia University, New York, New York 10027.

1. Lambert, L., Arm, M., "The Theory and Physical Constraints of an Electro-Optical Signal Processor for Phased Array Antennas," Technical Report T-1/199, October 1, 1963, Unclassified.
2. Aimette, A., Lambert, L., Arm, M., "Electro-Optical Signal Processing Techniques for Phased Array Antennas," Progress Report P-1/199, January 1, 1964, Unclassified.
3. Aimette, A., Arm, M., Brown, D., "Electro-Optical Signal Processing Techniques for Phased Array Antennas," Progress Report P-2/199, April 1, 1964, Unclassified.
4. Aimette, A., Arm, M., Wyman, N., "Electro-Optical Signal Processing Techniques for Phased Array Antennas," Progress Report P-3/199, July 1, 1964, Unclassified.
5. Aimette, A., Arm, M., Wyman, N., "Electro-Optical Signal Processing Techniques for Phased Array Antennas," Progress Report P-4/199, October 1, 1964, Unclassified.
6. Arm, M., Aimette, A., Lambert, L., Wyman, N., "Electro-Optical Signal Processing Techniques for Phased Array Antennas," Progress Report P-1/321, January 1, 1965, Unclassified.
7. Arm, M., Aimette, A., Lambert, L., "Electro-Optical Signal Processing Techniques for Phased Array Antennas," Progress Report P-2/321, April 1, 1965, Unclassified.
8. Lambert, L., "Electro-Optical Signal Processors for Array Antennas," Technical Report T-1/321, May 2, 1965, Unclassified.
9. Selected Semiconductor Circuits Handbook No. bsr 73231 Navships 93484, Pages 10-19.

COLUMBIA UNIVERSITY—ELECTRONICS RESEARCH LABORATORIES

10. Gibbons, J. F., and Horn, H. S., "A Circuit with Logarithmic Transfer Response over 9 Decades," IEEE Trans. Circuit Theory, September 1964.
11. Gray, J. R., and Kiktopoulos, S. C., "A Precision Sample and Hold Circuit with Subnanosecond Switching," IEEE Trans. Circuit Theory, September 1964.